Flood, R.D., Piper, D.J.W., Klaus, A., and Peterson, L.C. (Eds.), 1997
Proceedings of the Ocean Drilling Program, Scientific Results, Vol. 155

*6. MASS-TRANSPORT DEPOSITS OF THE AMAZON FAN[1]

D.J.W. Piper,[2] C. Pirmez,[3] P. L. Manley,[4] D. Long,[5] R.D. Flood,[6] W.R. Normark,[7] and W. Showers[8]

ABSTRACT

Seismic reflection profiles show at least four major mass-transport deposits (MTDs) on the Amazon Fan that drilling has shown date from the late Pleistocene. Each deposit extends over an area on the order of 10^4 km^2 and is 50–100 m thick. The entire thickness of individual MTDs was penetrated at Sites 931, 933, 935, 936, 941, and 944, and wireline logs were collected at most of these sites. Most deposits consist of large deformed blocks (meters to decameters) of clayey sediment. A little matrix is recognized between blocks, and some weaker smaller blocks are highly deformed. Thin matrix-rich deposits with small clasts near the top of some units are true debris flows. Properties of clasts in the MTDs show a broadly repetitive character vertically within the deposit, on a scale of meters to tens of meters. There is no evidence that a long time span is represented by discontinuities in sediment properties; rather, this repetitive pattern probably represents retrogressive failure from a headwall scarp. Major units 20–50 m thick within the MTDs can be correlated between sites. Sediment properties and microfossils suggest that most sediment was derived from muddy channel-levee deposits on the continental slope, but some sediment (particularly near the base of flows) resembles local deep-water levee sediments. Mass-transport events are inferred to have initiated in slope and upper-fan levee sediments. This sediment was underconsolidated because of rapid prodeltaic deposition during marine lowstands as well as a result of the presence of shallow gas and gas hydrates. Local steepening and weakening by diapiric intrusion may also have facilitated failure. The ages of the mass-transport events may correlate with times of falling sea level, when gas hydrate sublimation could destabilize sediments. MTDs were partly confined by pre-existing channel-levee topography on the fan. In places, high-relief levee deposits were eroded by the mass-transport flow and incorporated in the basal part of the deposit.

INTRODUCTION

Major blocky mass-transport deposits (MTDs) covering areas of hundreds of square kilometers, have been recognized as major components of continental margins from the past two decades of seafloor mapping with high-resolution seismic-reflection profiling and side-scan sonar (e.g., Walker and Massingill, 1970; Jacobi, 1976; Embley and Jacobi, 1986; Kenyon, 1987; Bugge et al., 1988; Lee, 1989). The surficial parts of only a few such deposits have been investigated in detail by acoustic imaging and coring (e.g., Normark and Gutmacher, 1988; Masson et al., 1993), but interpretation of their dynamics remains speculative (Hampton et al., 1996) in the absence of lithologic and structural detail about the deeper parts of these thick deposits. Although many of these MTDs have been loosely referred to as debris flows, other processes have been important in their formation and transport in many cases, and many show similarities to terrestrial landslides. The imprecise use of terminology results from both the commonly structureless character of the deposits on acoustic-reflection profiles, the lack of samples, and because failures may incorporate elements of both slides and debris flows. The entire thickness of major MTDs was penetrated at six different sites on Leg 155, thus providing important new insights into the character, origin, and transport processes of such deposits.

On the Amazon Fan (Fig. 1), MTDs are intercalated with thick, predominantly muddy levee deposits (Fig. 2). Individual levee units, which rapidly prograde downfan following turbidity-current channel avulsion, are grouped into larger levee complexes, each of which appears to correspond to a major lowstand in sea level (Flood, Piper, Klaus, et al., 1995, see "Leg Synthesis"). Two surficial MTDs are termed the Eastern and Western "debris flows" in recent publications (e.g., Manley and Flood, 1988). Each covers an area extending ~200 km downslope by 100 km in width, and each is 100–200 ms thick. Note that Damuth and Embley (1981) originally referred to Western "debris flow" as the "Central slump/debris flow complex" and applied the term western to the complex on the rise at 50°W (which we refer to as the 50°W MTD). The Western Mass-transport Deposit (WMTD) was cored at Site 941, whereas the Eastern Mass-transport Deposit (EMTD) was not sampled on Leg 155. A widespread buried MTD, the "Unit R Debris Flow" of Manley and Flood (1988) or Unit R Mass-transport Deposit (URMTD) of this paper, underlies the Upper Levee Complex (isotopic Stages 2–4) and was cored at Sites 935, 936, and 944. The correlative interval was penetrated downfan at Site 946, where sediment comprises thickly bedded sand with thin silt and mud beds. An MTD at the bottom of Hole 930C underlying the Orange Channel-levee Complex may be part of the URMTD, although this is not demonstrated by seismic-reflection correlation. On the eastern fan, an MTD overlying the crest of the Bottom Levee Complex (isotopic Stage 8) was cored at Sites 931 and 933; it is referred to here as the Bottom Mass-transport Deposit (BMTD). (We use this inelegant terminology because the MTD immediately overlies the so-called Bottom Levee Complex of Flood et al., 1991).

The historical nomenclature of marine MTDs is potentially confusing. In this paper, we generally follow the usage of Varnes (1978) and Nardin et al. (1979) in which the terms slide, slump, and debris flow each indicate a particular transport process. We use the term "mass-transport deposit" in a more general sense or where more than one process is involved. The characters of submarine slides and debris flows were originally defined using 3.5-kHz high-resolution reflection profiles (Jacobi, 1976) and have been refined as side-looking sonar and core data became available (Prior et al., 1984; Normark and Gutmacher, 1988; Normark, 1990). A slide involves displacement

[1]Flood, R.D., Piper, D.J.W., Klaus, A., and Peterson, L.C. (Eds.), 1997. *Proc. ODP, Sci. Results*, 155: College Station, TX (Ocean Drilling Program).

[2]Atlantic Geoscience Centre, Geological Survey of Canada (Atlantic), Bedford Institute of Oceanography, P.O. Box 1006, Dartmouth, N.S., B2Y 4A2, Canada. piper@agc.bio.ns.ca

[3]Lamont-Doherty Earth Observatory, Columbia University, Palisades, NY 10963, U.S.A.

[4]Geology Department, Middlebury College, Middlebury, VT 05753, U.S.A.

[5]British Geological Survey, West Mains Road, Edinburgh EH9 3LA, United Kingdom.

[6]Marine Sciences Research Center, State University of New York, Stony Brook, NY 11794-5000, U.S.A.

[7]U.S. Geological Survey, MS-919, 345 Middlefield Road, Menlo Park, CA 94025, U.S.A.

[8]Department of Marine, Earth and Atmospheric Sciences, North Carolina State University, 1125 Jordan Hall, Box 8208, Raleigh, NC 27695, U.S.A.

Previous Chapter Table of Contents Next Chapter

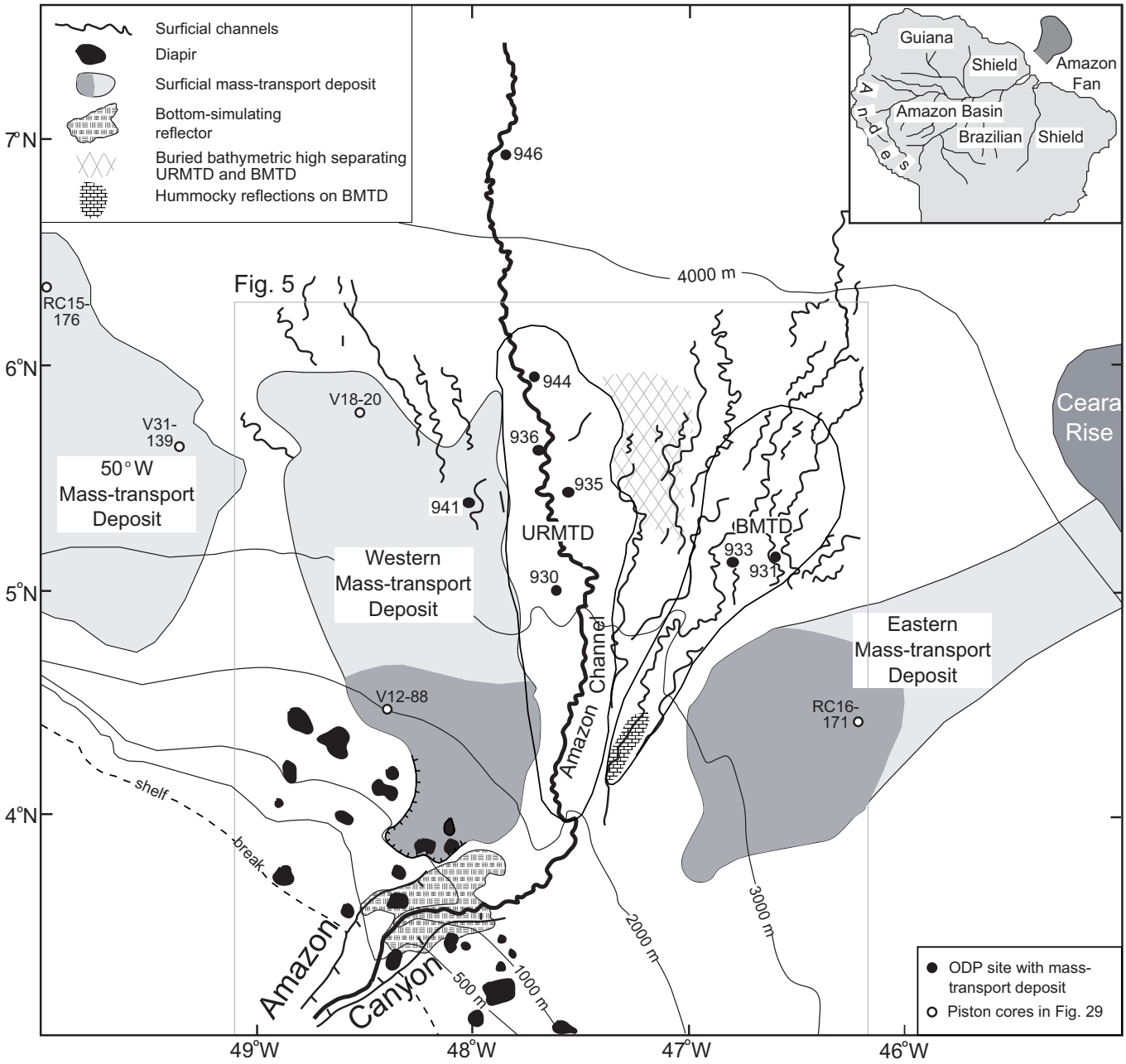

Figure 1. Map of the Amazon Fan showing location and character of surficial MTDs and the two major buried MTDs (URMTD = Unit R Mass-transport Deposit; BMTD = Bottom Mass-transport Deposit). ODP sites penetrating MTDs and piston cores illustrated in Figure 29 are also shown. Map modified from Damuth et al. (1988) and Manley and Flood (1988).

(shear) along defined shear surfaces. A slump is a particular form of slide in which there is rotational movement on shear surfaces: many slumps on the continental slope have moved only short distances and preserve back-tilted benches. Debris flows may develop from slides as a result of break up of blocks along multiple shear surfaces, internal deformation of blocks, and inmixing of seawater. Acoustic profiles of slides may reveal the presence of component blocks (Prior et al., 1984; Normark, 1990). The size of the blocks commonly decreases downslope, and slide deposits may merge downslope with structureless, acoustically transparent deposits with low surface relief but steep margins that are interpreted as a debris flows on seismic-reflection profiles. This gradation in acoustic properties from slides to debris flow deposits has resulted in both terms being used almost interchangeably in previous studies. In ancient deposits, lithologic features can be used to infer transport process. Debris flow deposits are mud-clast conglomerates, commonly with scattered pebbles and rafted blocks (e.g., Piper et al., 1978), whereas slide deposits comprise large blocks of sediment with deformation concentrated at their leading edge (Coniglio, 1986). Deposits that include elements of both slides and debris flows are also found. Some submarine slides and debris flows are thought to produce turbidity currents (Middleton and Hampton, 1976) as the mass-wasted sediment continues to deform and lose cohesion during transport and water is entrained with the moving and deforming sediment.

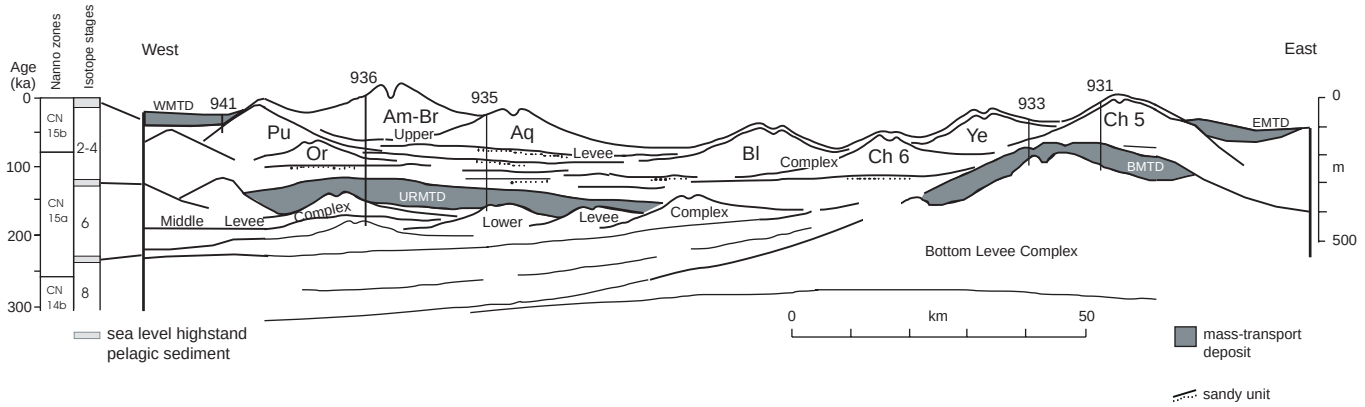

Figure 2. Schematic cross section of the Amazon Fan through selected ODP sites showing stratigraphic setting of the MTDs and stratigraphic correlation with isotopic stages and nannofossil stratigraphy. Names of turbidite systems (Ch 6, Ch 5, Or, Ye, Bl, Pu, Aq, Am-Br) are summarized in Table 1. Modified from Flood, Piper, Klaus, et al., 1995, "Leg Synthesis," fig. 1).

Purpose

This paper addresses three questions, based on seismic-reflection, core, and downhole logging data: (1) What is the age of the MTDs on the Amazon Fan? Does the age provide any insight into what triggered the mass-transport events, and was there any relationship to sea-level change? (2) What is the source area for the sediment in the MTDs? (3) What are the transport processes involved in the mass-transport events? Is each deposit a single or a multiple event?

The broader implications of each of these issues to the more general question of the origin of MTDs on continental margins are also considered.

Stratigraphic Nomenclature on the Amazon Fan

The Amazon Fan has aggraded principally by the deposition of thick levee deposits from a turbidity-current channel. Periodic channel avulsion has resulted in the deposition of a series of overlapping channel-levee deposits. Previous workers on the Amazon Fan have assigned color names to all the recognized channel-levee systems (Table 1; Fig. 2), with the exception of the youngest, which is termed the Amazon Channel-levee System, and two systems on the eastern fan, termed Channels "5" and "6." On the upper fan, upstream from any particular avulsion point, two successive channel-levee systems may be contiguous, as is the case of the Amazon and preceding Brown levee in Figure 2. Individual channel-levee units have been grouped into larger levee complexes: the Upper, Middle, Lower, and Bottom levee complexes (Fig. 2).

The proportion of sheet sands increases downfan. Sandy units interbedded with channel-levee systems appear as high-amplitude reflection packets (HARPs) on seismic reflection profiles. They were interpreted by Flood et al. (1991) as the first turbidite deposits following an avulsion, across which the new channel-levee system prograded. HARPs are thus assigned the same color names as the overlying channel-levee deposits (Fig. 3).

Chronologic control for this stratigraphic sequence is discussed elsewhere in this volume. Briefly, foraminifers, oxygen isotopes, and paleomagnetic data provide chronology for shallow continuously sedimented sequences. Important markers are the downcore reappearance of the foraminifer *Pulleniatina obliquiloculata* at ~40 ka (Maslin et al., this volume), the Lake Mungo paleomagnetic excursion at 32 ka (Cisowski and Hall, this volume) and the heavy isotope peak of the last glacial maximum at 18 ka (Showers et al., this volume). Interglacial deposits are lithologically distinct, consisting of hemipelagic calcareous clay, and contain distinctive warm foraminifer assemblages. These deposits can be assigned to nannofossil Zones CN15b (0–85 ka), CN15a (85–260 ka) and CN14b (260–460 ka), although the presence or absence of diagnostic species may be influenced by paleoenvironmental conditions (Maslin and Mikkelsen, this volume). The presence of isotope Stage 5 deposits at Sites 942 and 946 was confirmed by the presence of the Blake paleomagnetic event.

Table 1. Summary of stratigraphic nomenclature of the Amazon Fan.

Upper Levee Complex
Amazon (Am)
Brown (Br)
Aqua (Aq)
Purple (Pu)
Blue (Bl)
Yellow (Ye)
Channel "5" (Ch 5)
Orange (Or)
Channel "6" (Ch 6)
URMTD and BMTD
Middle Levee Complex
Red (Re)
Lower Levee Complex
Gold (Go)
Green (Gr)
Lime
Gray
Bottom Levee Complex

Note: From Damuth et al. (1983) and Manley and Flood (1988).

DISTRIBUTION

Surficial Mass-Transport Deposits

The EMTDs and WMTDs have been mapped from GLORIA long-range sidescan sonar, 3.5-kHz, and seismic-reflection profiles. Damuth and Embley (1981) described the 3.5-kHz acoustic echocharacter of these surficial "slump/debris flow complexes" on the fan. The upslope portion of the WMTD (their "central debris flow") shows a hummocky acoustic echocharacter (darker tone in Fig. 1), and they interpreted the region bounded by scarps between 700 and 1500 meters below sea level (mbsl) as a zone of slumping and sediment removal. The head of the WMTD is bounded by scarps up to 200 m high, forming a 15- to 25-km-wide valley subparallel to the

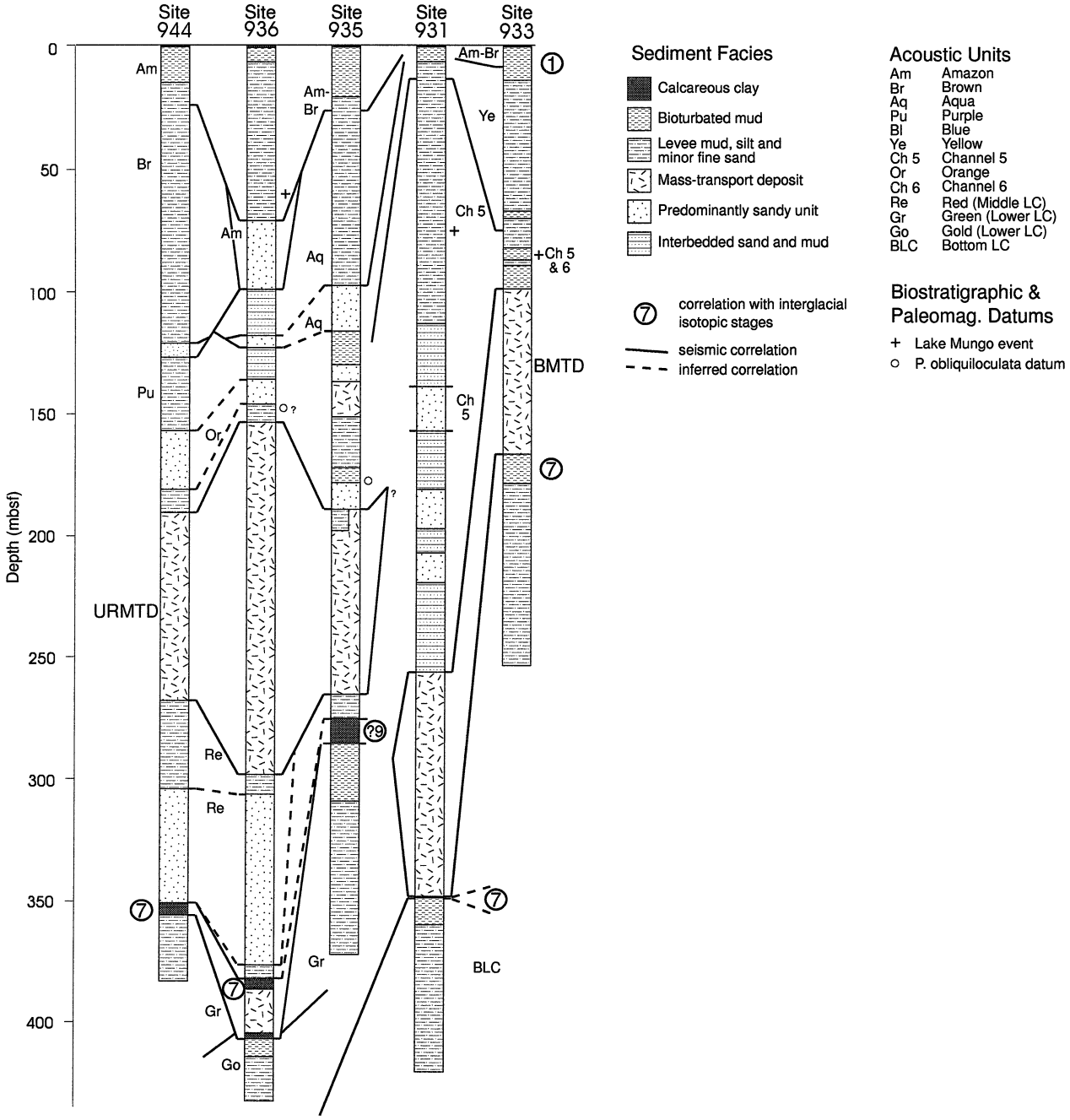

Figure 3. Stratigraphic sections of all sites penetrating buried MTDs showing key stratigraphic markers.

Amazon Canyon (Fig. 1). Lenses of acoustically transparent material up to 75 m thick occur within this valley (Damuth and Embley, 1981). Downslope, the WMTD has a smoother surface, although locally with hummocky relief of 5–10 m. Within the WMTD, Damuth and Embley (1981) noted patches of acoustically layered material, which they interpreted as turbidity current deposits generated at the same time or after the mass-flow event. In the vicinity of Site 941 (at 3400 mbsl), the deposit has a blocky surface with ~5 m of relief. Downslope, blocks appear to be larger (10–15 m relief) before an abrupt diminution in thickness with a concave up profile and a transparent acoustic character to a distinct snout at 3600 mbsl (Flood, Piper, Klaus, et al., 1995, "Site 941" chapter, fig. 4).

Seismic-reflection data from the WMTD indicate that scarps bounding the zone of sediment removal are associated with deformation resulting from rising diapirs or other deformations caused by large-scale gravity tectonics (Figs. 4, 5). Immediately south of the scarps, Manley and Flood (1988) identified a bottom-simulating reflection (Fig. 1), suggesting the presence of gas hydrates. A wedge-shaped body of relatively low acoustic amplitude in the scar area is interpreted as an old channel-levee system that was disrupted by the piercing diapirs. Seismic-reflection data show that the WMTD has a distinct eastern edge, abruptly terminating with a steep ramp against the low slope of Amazon Channel levee (Figs. 1, 6C, E). Seismic-reflection data show that the upslope part of the WMTD overlies the

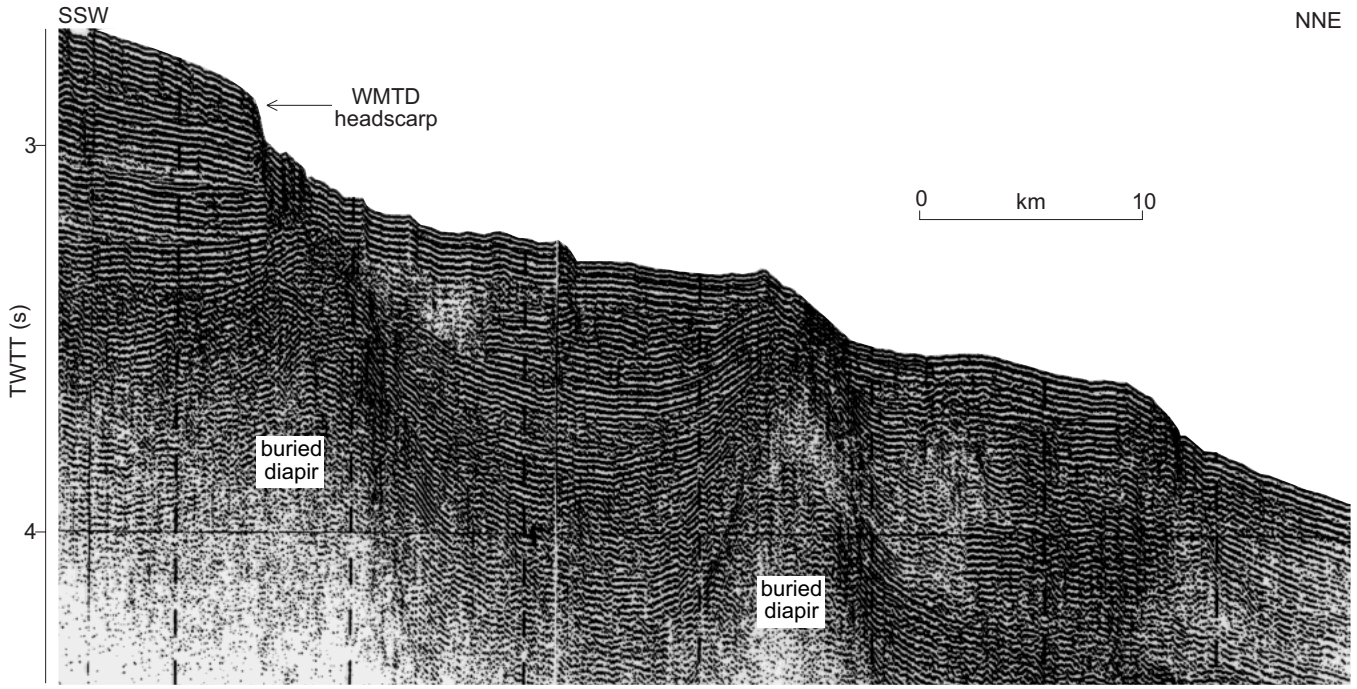

Figure 4. Longitudinal seismic-reflection profile of the upper part of the WMTD, showing the headscarp and relationship to buried diapirs. (Farnella 81-5, 10 January 1982, 0200–0530). Profile located in Figure 5.

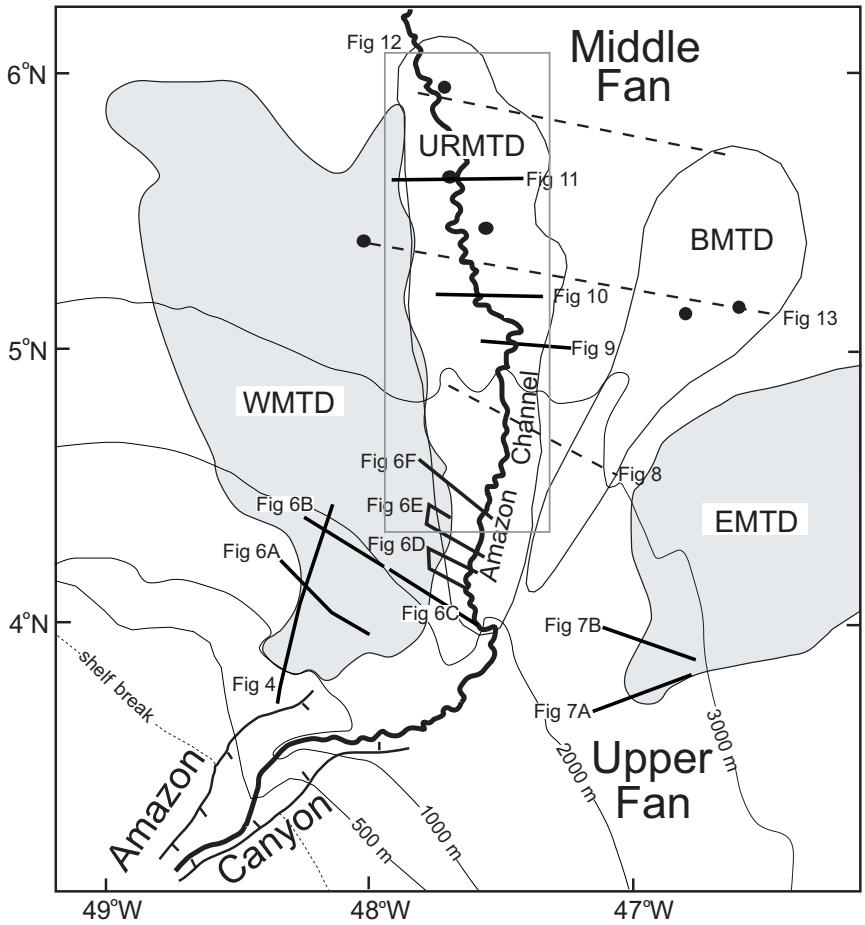

Figure 5. Map showing location of seismic profiles illustrated in this paper. Dashed lines are those profiles used to identify regional extent of the BMTD and URMTD.

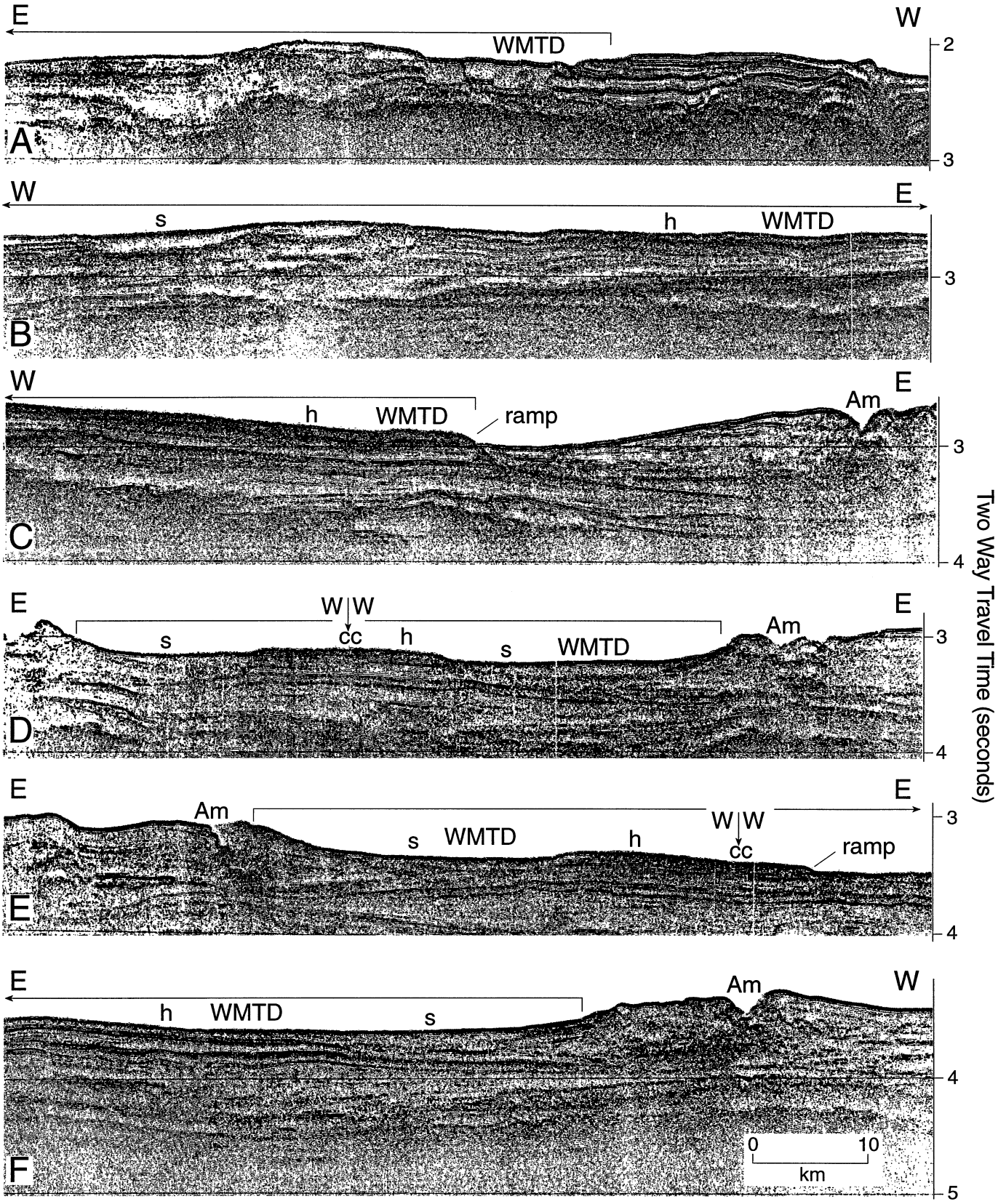

Figure 6. Series of strike (slope-parallel) seismic-reflection profiles illustrating the eastern margin of the WMTD. Profiles located in Figure 5. h = hummocky; s = smooth; Am = Amazon Channel; cc = change course. Horizontal line indicates extent of the WMTD.

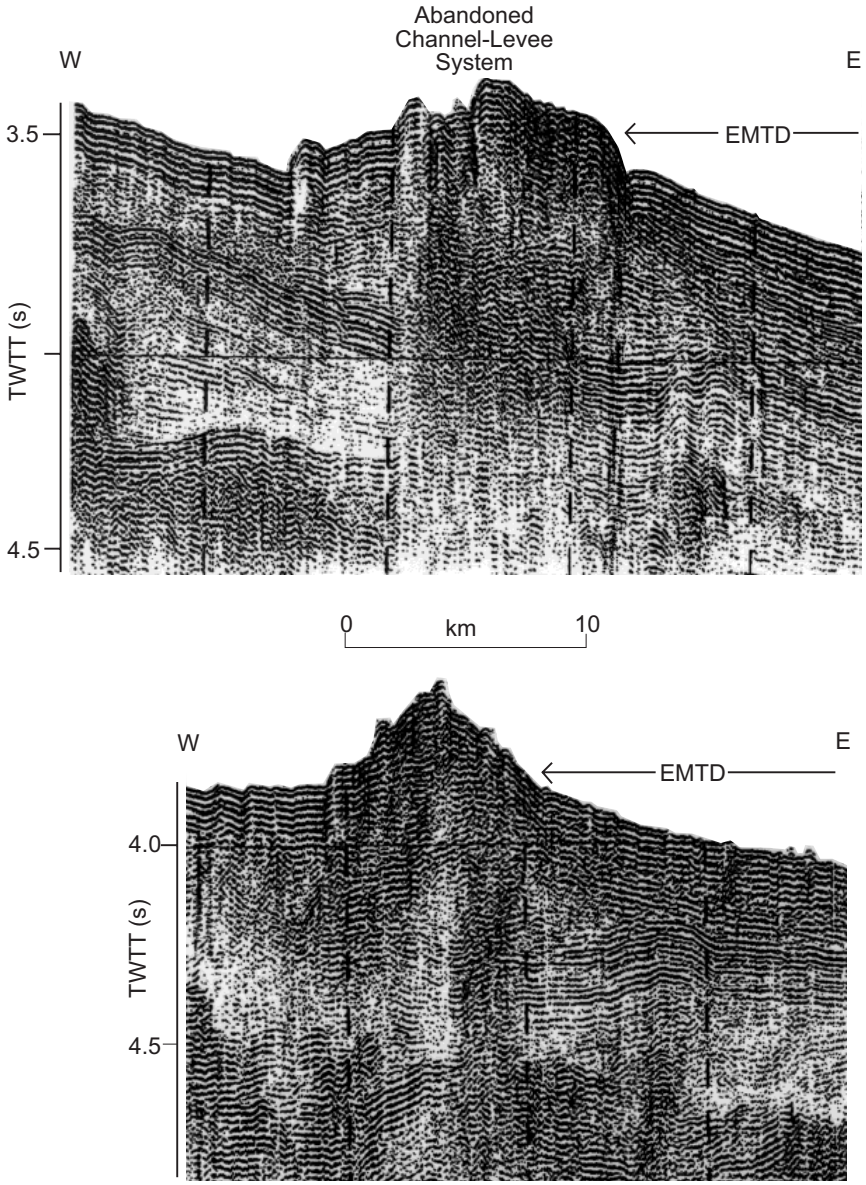

Figure 7. Two seismic-reflection profiles across the western margin of the EMTD, showing the bounding ridge near the upper limit of the deposit (Farnella 81-5, 0815–1015 and 1200–1400 UCT, 11 January 1982). Profiles located in Figure 5.

Amazon Channel-levee System (Pirmez, 1994, p. 352). On the downslope part of the WMTD, high-frequency 3.5-kHz reflection profiles show a thin veneer of sediment with parallel reflectors that thins westward from the distal end of Amazon Channel above the WMTD (Pirmez, 1994, p. 400–401). This veneer indicates that the WMTD was emplaced during the late stages of activity within the Amazon Channel, and may possibly represent several overbank depositional events. The WMTD has a maximum thickness of ~150 m, and the deposit is at least 100 m thick over much of its extent. Total volume is approximately 2000 km^3. The volume of "missing" sediment in the zone of sediment removal is perhaps 500–800 km^3, suggesting that sediment has also been eroded from beneath the WMTD. The deposit tends to bury underlying topographic irregularities, such as valleys between channel-levee systems (Fig. 4; see also fig. 19 of Damuth et al., 1988), and the surface of the WMTD rises only slightly over topographic highs. Apparent "overflow" from one valley to the next is probably a consequence of parallel flow down both valleys and spillover at valley bends.

The EMTD mapped on the fan surface by Damuth and Embley (1981) also has a zone of sediment removal associated with an ancient channel-levee system (Fig. 7A). The upslope part of the EMTD, shallower than 3400 mbsl, is characterized by hummocky topography, observed as overlapping hyperbolae on 3.5-kHz reflection profiles. Unlike the WMTD, no clear erosional headscarp is recognized in acoustic profiles; rather, the upslope limit of this zone is characterized by a sinuous, westward-facing steep slope of stratified sediment that represents an old levee crest (Fig. 7B). Seismic-reflection data across this area show a triangular-shaped wedge, which is acoustically semi-transparent, suggesting that the material in the EMTD originated from failure of the eastern levee of this old channel system. The deposits downslope from 3400 mbsl are acoustically transparent and laterally thin gradually over the underlying fan sediment. The blocky surface of the EMTD in 3.5-kHz profiles can be recognized at least to the 3700 m isobath. On GLORIA sonographs, the deposit appears more blocky than the WMTD. It is difficult to determine thickness from available seismic data, so the total volume can only be estimated as ~1500 km^3.

Buried Mass-Transport Deposits

Buried MTDs are recognized regionally from seismic-reflection profiles and include the URMTD and the BMTD. The URMTD ex-

tends over a large area of the present central Amazon Fan. The initial interpretation of aerial distribution of the Unit R deposit and estimates of its volume by Manley and Flood (1988) are inaccurate, because they included those deposits that are now identified as the BMTD (Manley and Flood, 1988).

Recently obtained seismic-reflection profiles (Figs. 8–11) allowed reevaluation of the earlier data to delineate the boundaries of the URMTD and the BMTD (Fig. 1). The upfan limit of the URMTD is near the 2000 m isobath, which is 50 km farther than previously published. There are uncertainties in the interpretation of these buried MTDs in seismic-reflection profiles, because locally the dipping levee sequences and MTDs have rather similar acoustic character (Fig. 9). The interpretations shown in seismic profiles and the isopach map (Fig. 12) represent the maximum extent of the URMTD. A more conservative interpretation would identify some of the thick deposits assigned to the eastern part of URMTD (e.g., the central part of Fig. 9) as levee deposits overlying HARPs that are interpreted as sand sheets by Flood et al. (1991). Given this interpretative uncertainty, some care must be used in drawing far-reaching inferences from seismic-reflection data from the buried MTDs. In general, the URMTD tends to have a nearly flat top with a irregularly shaped base where it fills topographic lows. It is characterized on acoustic profiles as a semi-transparent to chaotic acoustic facies with some coherent reflections within it (Manley and Flood, 1988; Pirmez, 1994). The URMTD is thinnest along its western boundary, which can be approximated by the eastern edge of the surficial WMTD. It wedges out and overlies the Lower Levee Complex or the Middle Levee Complex along this western boundary. It thickens to the east (Fig. 9), and the eastern boundary is approximated by the Blue Channel, although on the upper fan, the MTD is observed locally to extend eastward of the Blue Channel axis. The URMTD thins or is absent near the vicinity of the axis of the underlying Green levee system of the Lower Levee Complex. On the midfan, where the URMTD thickens to the east, it abruptly changes acoustic character from semi-transparent to a coherent set of parallel to subparallel reflections, and appears similar to a HARP (eastern part of seismic profile in Fig. 9). This abrupt change has been interpreted to be an apparent fault (Pirmez, 1994), but it could alternatively be the result of extensive erosion of

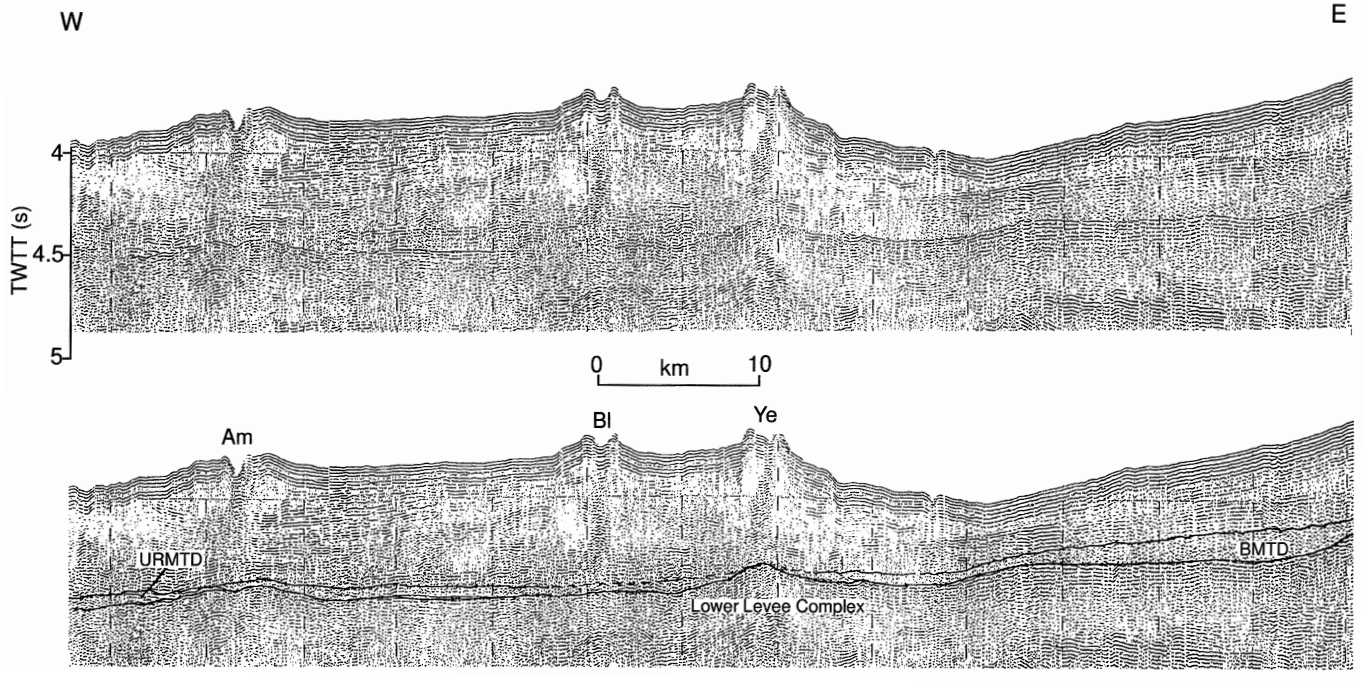

Figure 8. Slope-parallel single-channel reflection profile across the upper fan showing the possible connection of the URMTD and BMTD. Profile located in Figure 5. (Farnella 0430–1130 UCT, 12 January).

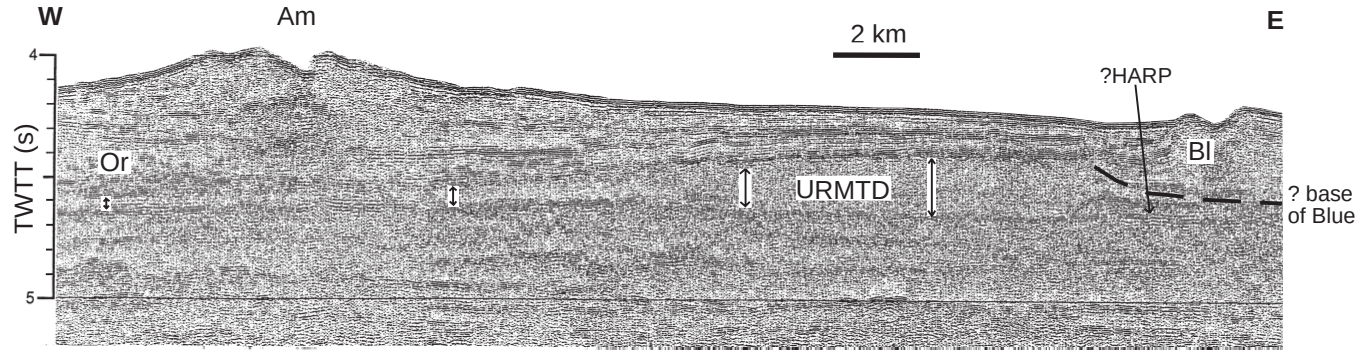

Figure 9. Seismic-reflection profile across upper fan (Line 1 of Pirmez, 1994), showing distribution of the URMTD (double arrows) and possible interpretations of the relationship between the URMTD and the Blue Channel-levee System. Dashed line shows base of Blue Channel-levee System from Pirmez (1994), but underlying HARP may be part of the same system. Am = Amazon, Bl = Blue, Or = Orange Channel-levee System (cf. Table 1). Profile located in Figure 5.

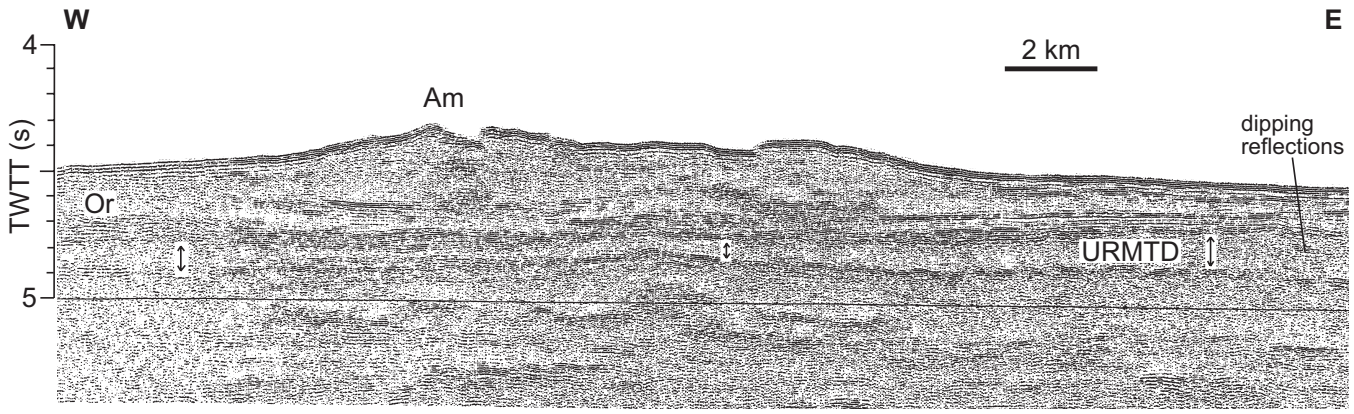

Figure 10. Seismic-reflection profile showing distribution of URMTD (double arrows) on the middle fan (Line 3 of Pirmez, 1994). Dipping reflections may be part of channel-levee system or may be allochthonous blocks. Am = Amazon, Or = Orange Channel-levee System. Profile located in Figure 5.

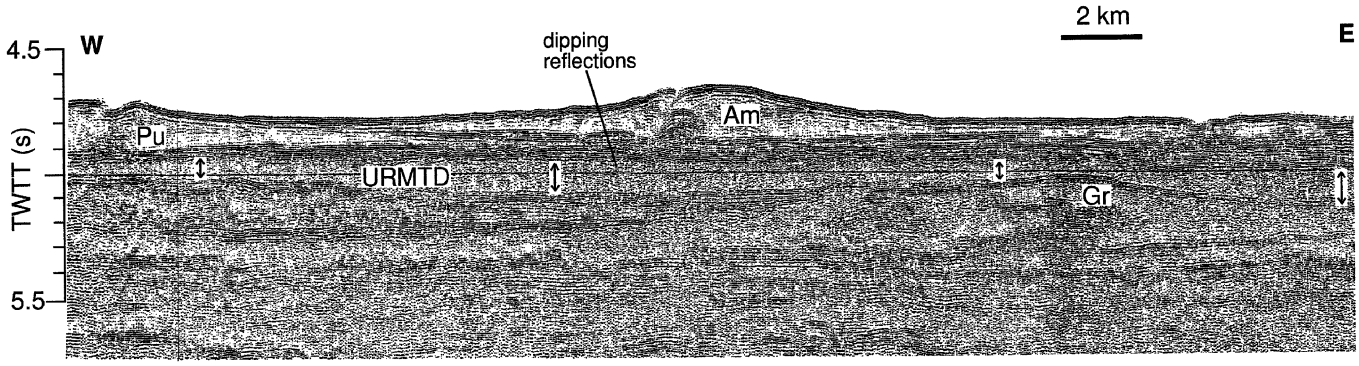

Figure 11. Seismic-reflection profile showing distribution of the URMTD (double arrows) across lower middle fan (Line 7 of Pirmez, 1994). Am = Amazon, Pu = Purple, Gr = Green Channel-levee System. Profile located in Figure 5.

URMTD when the Blue Channel prograded into this area (see below). Progressively farther downfan, URMTD still thickens to the east, but it appears to merge with levees of the Orange 2 (Figs. 10, 11) or in some places, the Blue Channel system. Near the lower part of the fan, URMTD thickens to the east and again merges with HARP-like deposits, which appear to be related to the Blue Channel-levee System (Fig. 13). The URMTD extends over $\approx 11 \times 10^3$ km^2 and has a volume of ~610 km^3.

The BMTD overlies the Bottom Levee Complex. Its aerial distribution is not as well constrained as the URMTD because of sparse seismic-reflection data. The acoustic facies of the BMTD are similar to the URMTD, mostly semi-transparent to chaotic in nature, flat topped and filling valleys between channel-levee systems. The western extent of the BMTD appears coincident with the Yellow Channel and the Blue HARP unit farther downfan (Figs. 1, 13). As was observed on the eastern edge of the URMTD, the BMTD on the middle fan is semi-transparent, thins, and merges abruptly into HARP-type reflections on its western edge. Its upfan extension appears to include a region of hummocky reflections near the 2000-m isobath (visible on Farnella 81-5, 4 January 1982, 1430–1700: not illustrated here). These hummocky reflections could indicate the source of failure for this deposit or could be an acoustic characteristic of the Yellow Channel, as the seismic line is nearly directly over the channel within this region. The BMTD extends ≈200 km north from its source area on the continental slope. Pockets of apparent MTDs are observed farther downfan, but they cannot be directly correlated with the BMTD. The eastern extension of this unit is speculative. The main constraint is that it does exist ≈20 km east of Site 931 and is observed on a north-south seismic line just west of the surficial EMTD (Fig. 1).

The BMTD becomes very thin near Site 933 (Fig. 13), which is located just west of a region that is a highly reflective zone on GLORIA sidescan sonar imagery. This reflective zone correlates with a near-surface expression of a buried channel-levee belonging to the Bottom Levee Complex (≈120 meters below seafloor [mbsf]); see Fig. 13D), which produces a 100–150-m step in the bathymetry from east to west over a horizontal distance of 3.5 km. Seismic-reflection profiles obtained from the *JOIDES Resolution* (Flood, Piper, Klaus, et al., 1995, "Site 931" chapter, fig. 3) show a hummocky facies directly over this buried channel-levee. To the east of this step, the BMTD has a transparent facies averaging ≈120 m thick (sampled at Site 931), that can be traced laterally and downfan. To the west of the step, the unit thins dramatically to less than 60 m at Site 933 and then wedges out, being overlain by the Channel 6 levee of the Upper Levee Complex. The downfan limit of the BMTD is within the middle fan area and a first-order approximation of its areal extent is $\approx 7 \times 10^3$ km^2.

The question remains as to whether or not the URMTD and the BMTD are the same unit. Only three seismic-reflection lines running east-west are available to determine whether these two units are equivalent (Fig. 5). The two northern lines both demonstrate the thickening of the URMTD to the east and the thinning of the BMTD to the west into the area of HARP-type reflections. The southernmost line (Fig. 8) is near the upper reaches of the Blue Channel where the HARP unit is not well developed. This reflection profile suggests that these two MTDs may be the same, and Figure 12 shows a possible scenario relating deposition of these two MTDs. Prior to 40 ka (Piper et al., Chapter 39, this volume), the surface topography of the fan had two major bathymetric highs: the Bottom Levee Complex in the east

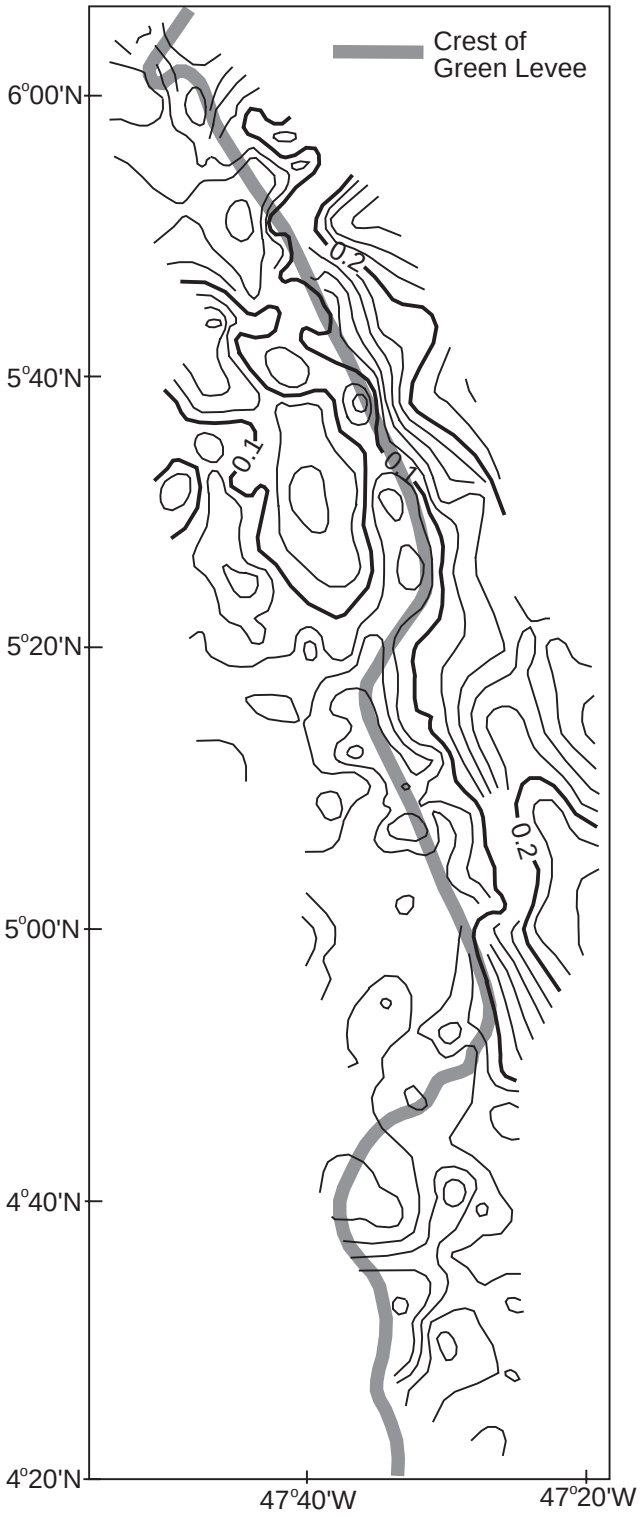

Figure 12. Isopach of the URMTD in two-way traveltime (in seconds). For location, see Figure 5. The URMTD is thickest to the east, reaching a maximum of 0.26 s. It is thinnest to the west and along the crest of the Green levee system (cf. Table 1). The gridding, visualization, and volumetric analysis of the URMTD data were accomplished through the use of Earth Visions software created by Dynamic Graphics Inc., Alameda, California.

and the Green levee of the Lower Levee Complex to the west (Fig. 13A), representing the last active channel-levee system for their respective levee complex. One or several mass-transport events initiated on the upper slope region flowed down between these bathymetric highs. Near the bathymetric highs, the mass-transport flow was either deflected away from or locally partially flowed over these features (Fig. 13B). The low of both sides of the channel-levee system of the Bottom Levee Complex ponded on the flanks of this bathymetric high with a thicker section preserved on the steeper eastern side than the western. Near the Green Channel-levee System of the Lower Levee Complex, the mass-transport flow was able to overflow the levee crest, but the deposit rapidly thinned to the west. As the Upper Levee Complex began to form, it developed on top of the MTD. When Channel 6 and Yellow Channels prograded across the lower middle fan, they eroded the MTD leaving only small pockets on the western side of the Bottom Levee Complex. The development of the Blue Channel farther to the west, where the MTD was thicker, removed some of the MTD by erosion (Fig. 13C). The HARP associated with the developing Blue system would have been limited laterally by the limits of this erosion. The subsequent development of the Blue levee over that HARP and merging with the URMTD would give the appearance of a thickening URMTD that abruptly changes into high-amplitude parallel reflections (Fig. 9). The lower resolution of some of the seismic-reflection profiles, however, prevents definitive resolution of the question of whether the two sampled MTDs (URMTD and BMTD) are the same. If these units are the same, then their emplacement was modulated by bottom topography, and they were subjected to subsequent modification by extensive erosion.

Evidence for Erosion Beneath Mass-Transport Deposits

In several areas, seismic-reflection profiles show local erosion beneath MTDs. At Site 935, the crest of the underlying levee appears to have been planed off (Flood, Piper, Klaus, et al., 1995, “Site 935” chapter, fig. 3). At Site 933, seismic-reflection profiles indicate that the surface of the Bottom Levee Complex is locally quite irregular (Flood, Piper, Klaus, et al., 1995, “Site 933” chapter, fig. 2), also suggesting possible erosion. A seismic-reflection profile at Site 941 (Flood, Piper, Klaus, et al., 1995, “Site 941” chapter, fig. 2) shows a very irregular base to the MTDs and the sediment of the underlying Purple Channel-levee System appears to be deformed.

Regionally, however, the base of the MTDs appears sharp in seismic-reflection profiles and shows little evidence for erosional truncation of underlying reflections, as shown in Figures 9–11 for the base of the URMTD. Locally, however, the URMTD terminates abruptly against pre-existing channel-levee sediments, for example in seismic Line 5 illustrated as fig. 16 of Pirmez and Flood (1995). We cannot agree on whether these abrupt contacts reflect ponding against pre-existing topography or whether they provide evidence for in situ failure contributing to the MTDs; probably both situations exist.

Summary

Observations summarized above on both surficial and buried MTDs deposits suggest the following general characteristics inferred from acoustic mapping data:

1. MTDs are derived from source areas in water depths of 500–2500 mbsl where there are thick channel-levee deposits. The continental slope to 1500 mbsl is cut by diapirs and in places shows bottom-simulating reflections.
2. The upslope parts of surficial MTDs appear very blocky on high-resolution acoustic profiles. Blockiness decreases downslope, but only the extreme distal parts of the deposits appear smooth.

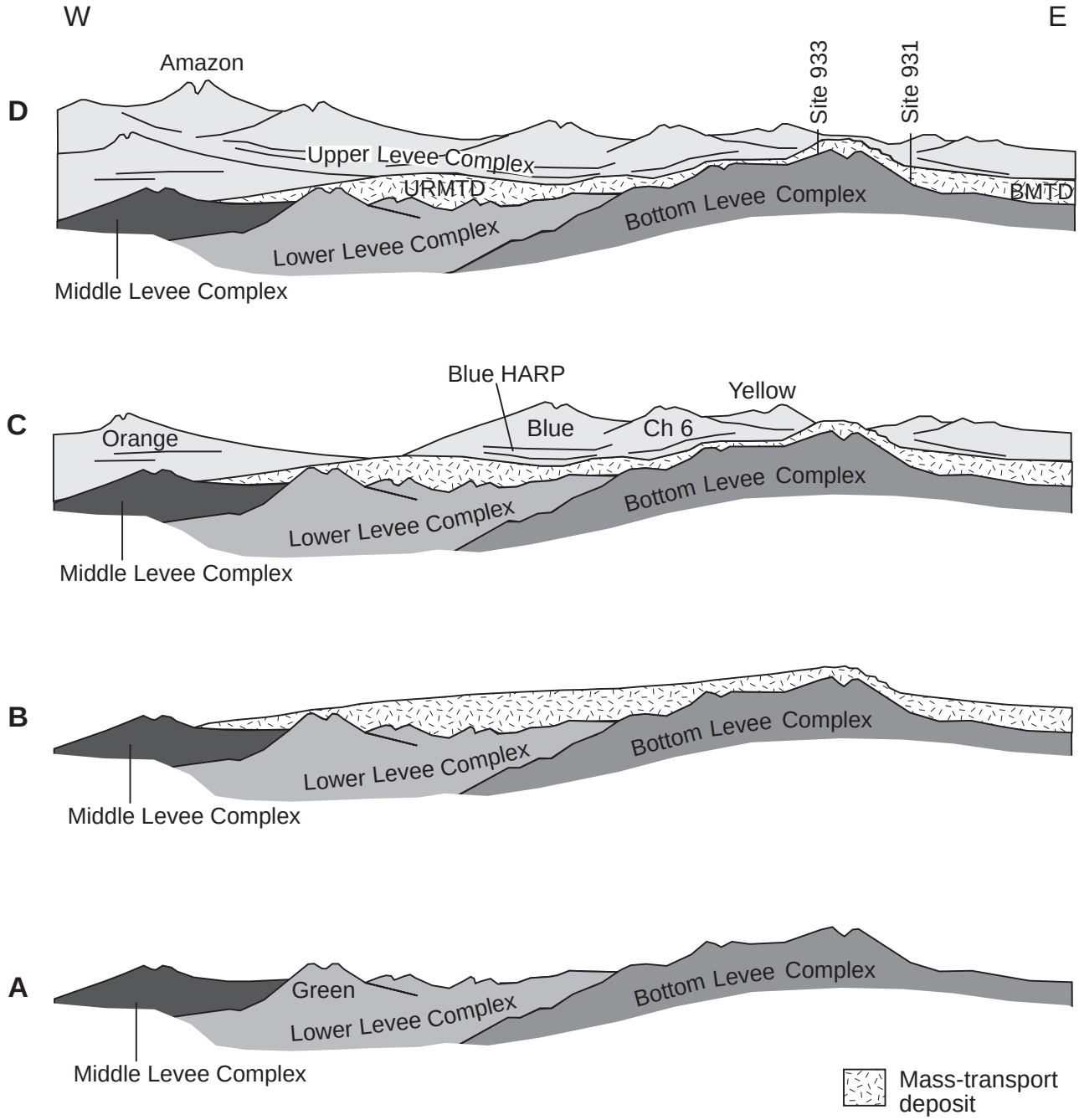

Figure 13. Schematic profiles across the middle fan showing the development of the URMTD and BMTD through time. Profile located in Figure 5. **A.** Fan morphology before the emplacement of the MTD. The Green Channel-levee of the Lower Levee Complex and the unnamed levee of the Bottom Levee Complex were two prominent bathymetric highs on the fan surface. **B.** Deposition of the MTD, which ponded between the two prominent bathymetric highs and thinned on the outer edges of these features. **C.** The emplacement of Channel 6 and Yellow Channel-levees eroded most of the MTD, leaving only small pockets. The emplacement of Blue Channel eroded part of the mass-transport unit and subsequently filled it with a sandy HARP unit associated with the Blue Channel. The Blue levee prograded over the HARP unit and overlies the mass transport unit, apparently thickening the URMTD to the east. **D**. Present-day Amazon Fan morphology based on seismic-reflection profiles and Leg 155 results.

3. As MTDs flowed downslope, they appear to have locally moved across the crests of channel-levee systems, but they generally fill valleys between channel-levee systems and have rather flat tops. The URMTD generally shows more surface relief than the surficial MTDs. Ridges formed by buried levee crests commonly mark the lateral boundaries of MTDs, but in places distinct lateral ramps are visible. Downfan, the margins of MTDs have been eroded during the deposition of HARPs associated with prograding channel-levee systems.
4. In places, seismic-reflection profiles indicate that the lower contact of MTDs is erosional. In particular, levee crests locally appear planed off. Analogous observations have been reported

in slides elsewhere (Trincardi and Normark, 1989). Lateral contacts of MTDs with older sediments may also show evidence for sediment failure.

LITHOLOGY

Introduction

Our interpretation of the character of the MTDs is based principally on description of the split core face and shipboard determinations of physical properties and microfossils. Detailed descriptions are available in the individual site chapters of Flood, Piper, Klaus, et al. (1995) and are not repeated here, but salient features are summarized in Figure 14 and Table 2. Downcore variations in these various parameters are compared with wireline logs, which are available for parts of the buried MTDs. Lithologic variability is determined from core descriptions of the split core face (Fig. 15), downcore variation in physical properties and microfossils, and from logging data. Characteristics of sediment source are provided by laboratory studies of sediment samples (e.g., grain size, geochemistry), microfossil content, and some physical properties. The Formation MicroScanner (FMS), which measures microresistivity of the borehole wall from four orthogonal pads with a resolution of <1 cm, has been particularly useful for analyzing the in situ character of the sediment and the deformation associated with the emplacement of the MTDs. In the FMS images in Figure 16, more resistive clasts and beds (typically of silt or sand) appear as a lighter tone. Correlation of a single bed between the four pads allows the dip and azimuth of bedding to be calculated (tabulated on the right-hand side of the images in Fig. 16). Many FMS images obtained during Leg 155 are degraded as a result of poor pad contact against a rugose borehole wall (Fig. 16E). Fortunately, over most of the intervals logged the images are of sufficient quality in at least one pad so that one can determine an electric facies that is closely related to the nature of bedding and grain size in the sediment (see Pirmez et al., this volume). Here, we present an initial analysis of the FMS images within the URMTD and BMTD intervals. In particular, we measured the orientation of numerous beds and bed boundaries and determined the depths at which abrupt changes of dip/azimuth occurred. The main objective is to make a preliminary assessment of deformation structures within the MTDs, which was not feasible with the core material alone on the ship.

Lithologic Variation Through Individual Mass-Transport Deposits

Most of the MTDs are inferred to consist of mud blocks with a variety of physical scales. These scales can be inferred from split core surface, although "biscuit" deformation (Flood, Piper, Klaus, et al., 1995, see "Explanatory Notes") makes this difficult in uniform textured sediment (Fig. 15C). Analysis of abrupt changes in dip/azimuth of bedding from FMS images allow block boundaries to be identified (Fig. 16A) and smaller blocks or clasts can be recognized in a single FMS image (Fig. 16B). In some cases, block size can be inferred from the uniformity of microfossil assemblages and from the continuity of index and strength properties (e.g., Fig. 17). Resistivity, gamma and other wireline log data (Figs. 18, 19) can also be used to infer block size and can be correlated with shipboard measurement of physical properties (Fig. 20). Such data show that block sizes locally are on the scale of centimeters (Figs. 15D, 16B), whereas elsewhere the recovered sediment appears relatively uniform over tens of meters of thickness, such as the basal part of the MTDs in Sites 933 (Fig. 19) and 936 (Fig. 20).

Although there is considerable small-scale variability, it is possible to classify the URMTD and BMTD into five main lithologies (Fig. 14):

1. Intervals of uniform mud typically 10–30 m thick with rather uniform characteristics (such as foraminifer content, magnetic susceptibility, or uranium content). This uniformity suggests that these intervals represent large blocks (Fig. 16A), of a scale similar to that inferred from 3.5-kHz profiles. In places, there are muddy or sandy intervals a few meters thick between these inferred blocks (Fig. 18). The large blocks locally show complete folds both in core section and FMS logs (Fig. 16E). They contain numerous small faults and evidence of shearing. In general, cores from intervals with large blocks lack obvious matrix material and such blocks have the highest strength properties and are found at or near the base of MTDs.
2. Intervals with uniform or gradational properties in muddy sediment on a scale of a few meters, as for example in unit B of the URMTD at Site 936 (Fig. 20) or the cyclical pattern noted at Site 941 (Fig. 17). Small folds are visible directly in FMS images (Fig. 16C) whereas larger folds can be detected from dip reversals (203.5 mbsf in Fig. 16D).
3. Intervals where the variability in split core surface, in logs, and in physical properties suggests blocks of sizes less than 1 m (Fig. 16B, F). This lithology is commoner in the upper part of the MTDs, but is also found at the base of the BMTD at Site 931 and at 253 mbsf at Site 935 (Fig. 14; Table 2).
4. Intervals with common sand were generally poorly recovered and borehole washout degraded log data (e.g., Fig. 16B; 260 mbsf in Hole 936A in Fig. 18).
5. Intervals (e.g., at the top of MTDs in Sites 931 and 935) where the sediment is distinctive because it appears highly folded and consists of mud with many silty laminae, in contrast to the more uniform muds elsewhere in the MTDs.

In places, the character of successive blocks appears repetitive. At Site 936, index property data and log data show five cycles from 170 to 225 mbsf (Fig. 20). At Site 941, there is an alternation of glacial and interglacial foraminiferal assemblages in the blocks, with lower water content in the interglacial sediments (Fig. 17). The buried URMTD and BMTD tend to have coarser sediment near the base and finer sediment higher in the deposit, with several fining-up cycles visible at Sites 935 and 936 (Manley et al., this volume).

Matrix material is generally difficult to identify in the split core face. Where small (<10 cm) clasts are present, a grey muddy matrix similar to the predominant block lithology is visible (m in Fig. 15E) that contains elongate color patches suggesting shear. Individual less compacted blocks appear deformed and penetrated by stronger blocks (e.g., at 99 cm in Fig. 15E, where block "c" penetrates lamination in the overlying deformed block). Matrix material may also be present between larger deformed blocks (e.g., at 67 cm in Fig. 15F). Overall, however, it is not possible to systematically identify matrix. In many cases individual blocks appear to be in direct contact with one another without intervening matrix (e.g., at 88 cm in Fig. 15D).

Deformation of Sediments

Because of coring disturbance associated with extended core barrel (XCB) coring of the buried MTDs on the Amazon Fan, the FMS microresistivity images obtained at Sites 935, 936, and 944 (for the URMTD) and at Site 933 (for the BMTD) are of particular importance in understanding the characteristics of the deformation associated with the emplacement of these deposits. During Leg 155, the XCB cores from the MTDs were commonly characterized as having "woodgrain" facies (Fig. 15C), which were tentatively interpreted as resulting from "biscuiting" of beds that dipped at various angles (Flood, Piper, Klaus, et al., 1995, see "Explanatory Notes"). This deformation severely handicapped the shipboard party from assessing the nature of the deformation within the MTDs.

The nature of the deformation within the URMTD and BMTD can be assessed by examining the changes in dip and azimuth of the sediment layers measured by the FMS. In many cases, beds dipping in one direction are superposed by beds dipping at 180°, suggesting the presence of folded structures (Fig. 16A). Multiple changes in azimuth

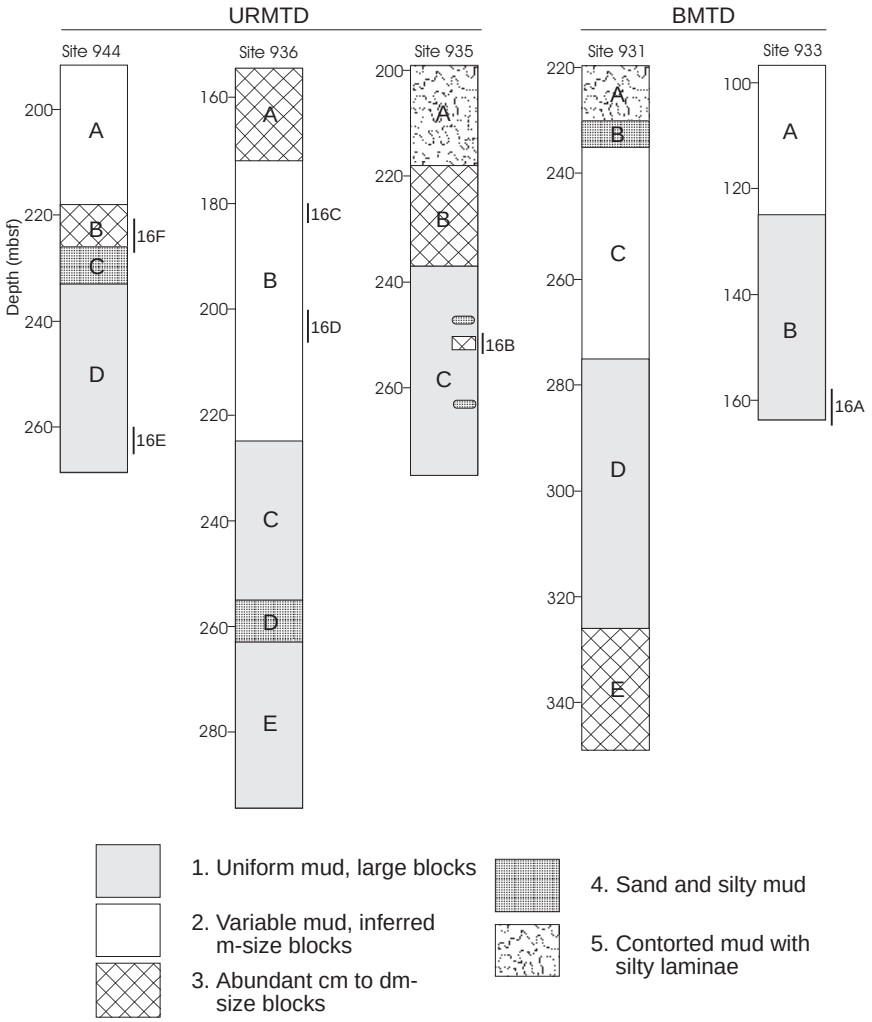

Figure 14. Lithologic interpretation of the URMTD and BMTD. Lithologies 1–5 are described in detail in text. A through E are units defined in Table 2. Small bars indicate location of images in Figure 16A through 16F.

Table 2. Subunits of mass-transport deposits.

Subunit	Depth (mbsf)	Distinctive properties
Hole 931A		
A	220–230	Folded blocks of mud with silt laminae. Common *P. obliquiloculata.*
B	230–235	Sandier interval, common mud clasts.
C	235–275	Large mud clasts. Plant fragments common. Scatter in index properties. *P. obliquiloculata* absent in most samples
D	275–326	Large mud clasts. At top, change in magnetic susceptibility and water content profile. Uniform index properties, break at 302 mbsf. *P. obliquiloculata* common in most samples.
E	326–349	Mud blocks with decimeter- and centimeter-sized clasts including carbonate-rich muds.
Hole 933A		
A	97–125	Mud with decimeter-sized clasts, some sand. No *P. obliquiloculata.* FMS shows change in average dip at 108 mbsf (Fig. 21A).
B	125–164.5	Large mud blocks. Lower magnetic susceptibility, higher U and higher N than in upper part of mass-transport deposit. *P. obliquiloculata* present. [Note that index properties (Fig. 27) and resistivity, velocity, porosity, and density logs (Fig. 19) show a change at 130–133 mbsf. FMS images show higher dips with higher scatter below this level (Fig. 21A)].
Hole 935A		
A	199–218	Folded blocks of mud with silt laminae. Common *P. obliquiloculata.*
B	218–237	Mud with decimeter- and centimeter-sized clasts, including carbonate-rich mud.
C	237–276	Large mud blocks, some sandier intervals, rare smaller clasts. Few *P. obliquiloculata* throughout.
Hole 936A		
A	154.5–? 172	Abundant decimeter- and centimeter-sized mud clasts, wood, shell fragments, and fine pebbles.
B	? 172–225	Large mud blocks. Five fining up cycles on gamma log, some corresponding water content profiles. *P. obliquiloculata* common in upper part, becoming rarer lower.
C	225–255	Large mud blocks. Abrupt increase in strength. Abundant bathyal foraminifers. *P. obliquiloculata* increases down-unit.
D	255–263	Sandier interval. Abundant *P. obliquiloculata*.
E	263–294	Large mud blocks. Highest resistivity and gamma. Bathyal foraminifers rare. Few *P. obliquiloculata.*
Hole 944A		
A	192–218	Mud blocks, folded, probably decimeter-sized. Rare smaller clasts. Rare bathyal foraminifers. No *P. obliquiloculata.*
B	218–226	Interval with common carbonate-rich and other decimeter-sized clasts.
C	226–233	Sandier interval.
D	233–268	Mud blocks. Different color from A. No bathyal foraminifers, but common *P. obliquiloculata.*

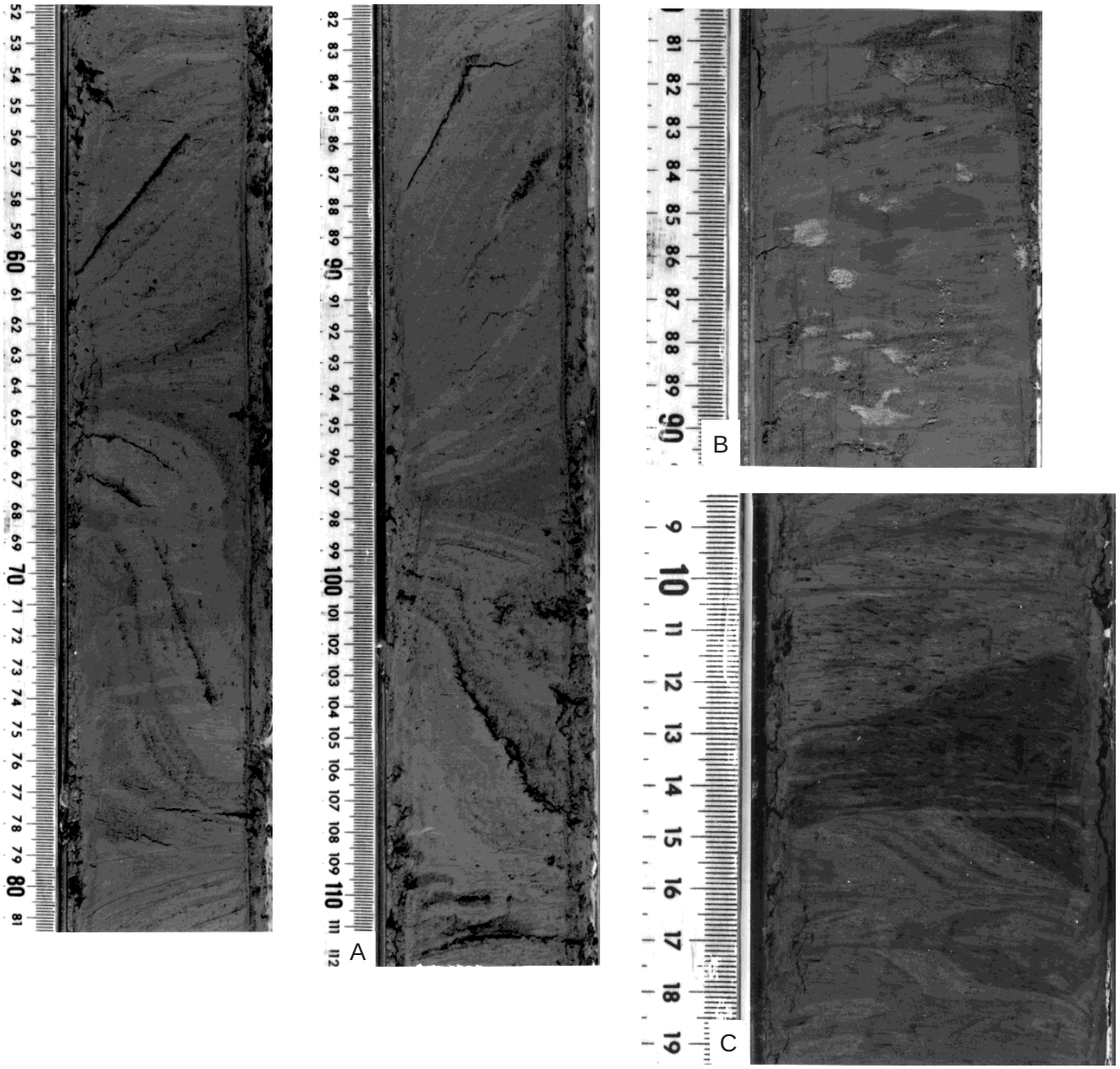

Figure 15. Core photographs of selected intervals. Photographs A–D are also imaged by FMS logs. **A.** Folded sediment, interval 155-933A-18X-1, 50–110 cm, probably corresponding to the upper part of Figure 16A. The lack of folding in the FMS image suggests that this folding results from drilling deformation, as interpreted by Flood, Piper, Klaus, et al. (1995, p. 211). **B.** Highly bioturbated sandy mud interval (Section 155-935A-28X-4) corresponding to a large block in Figure 16B. **C.** "Woodgrain texture" in muds from Section 155-936A-19X-6, resulting from biscuit rotation in folded blocks. This interval corresponds approximately to FMS image in Figure 16C.

direction probably indicate the presence of several blocks (Fig. 16E). Gradual changes in dip uphole are also observed, suggesting perhaps gentler folded structures or larger scale folds. Small-scale folding that could be observed within a single pad is rare (Fig. 16C). The apparent scarcity of small-scale folding would indicate that the sediment within the MTDs may have been too stiff to generate such small-scale folds, and it must have been transported as fairly large blocks, which were more or less coherent. Within some intervals, smaller blocks on a decimeter scale are visible (Figs. 16B, F) and correspond to rapid changes in lithology in recovered core (Fig. 15D). In Hole 933A, a highly folded core interval (Fig. 15A) was derived from an interval that shows no folding on FMS, confirming the shipboard interpretation that this particular folding resulted from drilling disturbance.

The MTDs differ from autochthonous channel-levee deposits in showing dips greater than 30° with azimuths that vary by up to 180° over short intervals. Dip-azimuth ("tadpole") plots for Holes 933A, 936A, and 944A are shown in Figures 21A through 21C. For Site 933, we show in addition a plot of the azimuth of measured beds vs. depth (Fig. 21D). In each of those plots, we marked apparent boundaries where either bed azimuth or dip changed significantly (greater than ~45° for azimuth). These boundaries separate zones where bed

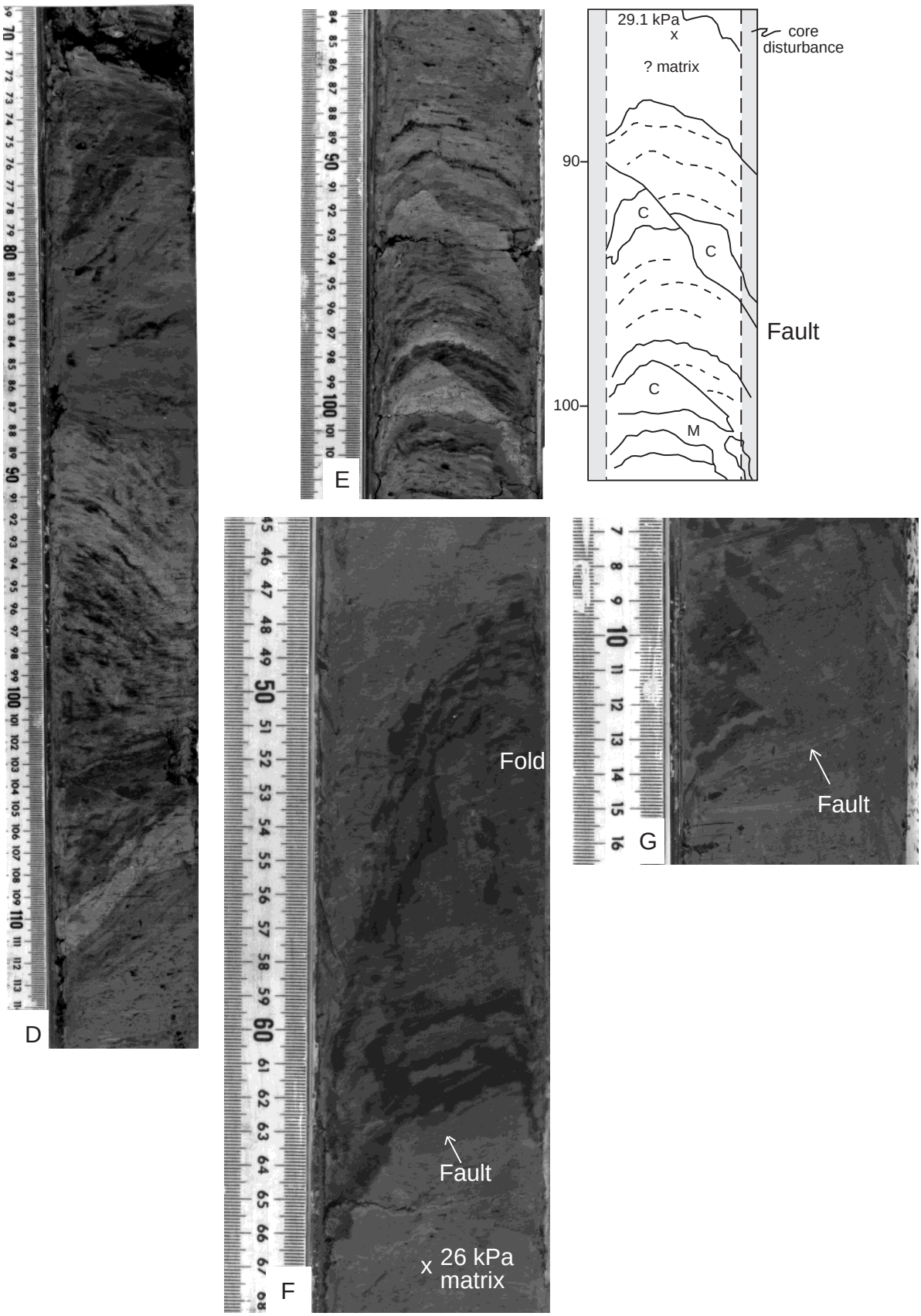

Figure 15 (continued). **D.** Several small clasts in Section 155-944A-25X-5. This interval is just below the image in Figure 16F. **E.** Photo and interpretation showing small clasts and probable matrix (M) in Section 155-941A-4H-5. Clasts include relatively rigid light-colored clasts with ≈5% $CaCO_3$ (C) and more deformed color-banded muds **F.** Photo of deformed color-banded mud blocks showing overall fold deformation and small-scale fault offset from Section 155-941A-3H-7. Underlying lighter mud may represent matrix. **G.** Series of small faults in color-banded mud clast from Section 155-941A-6H-3.

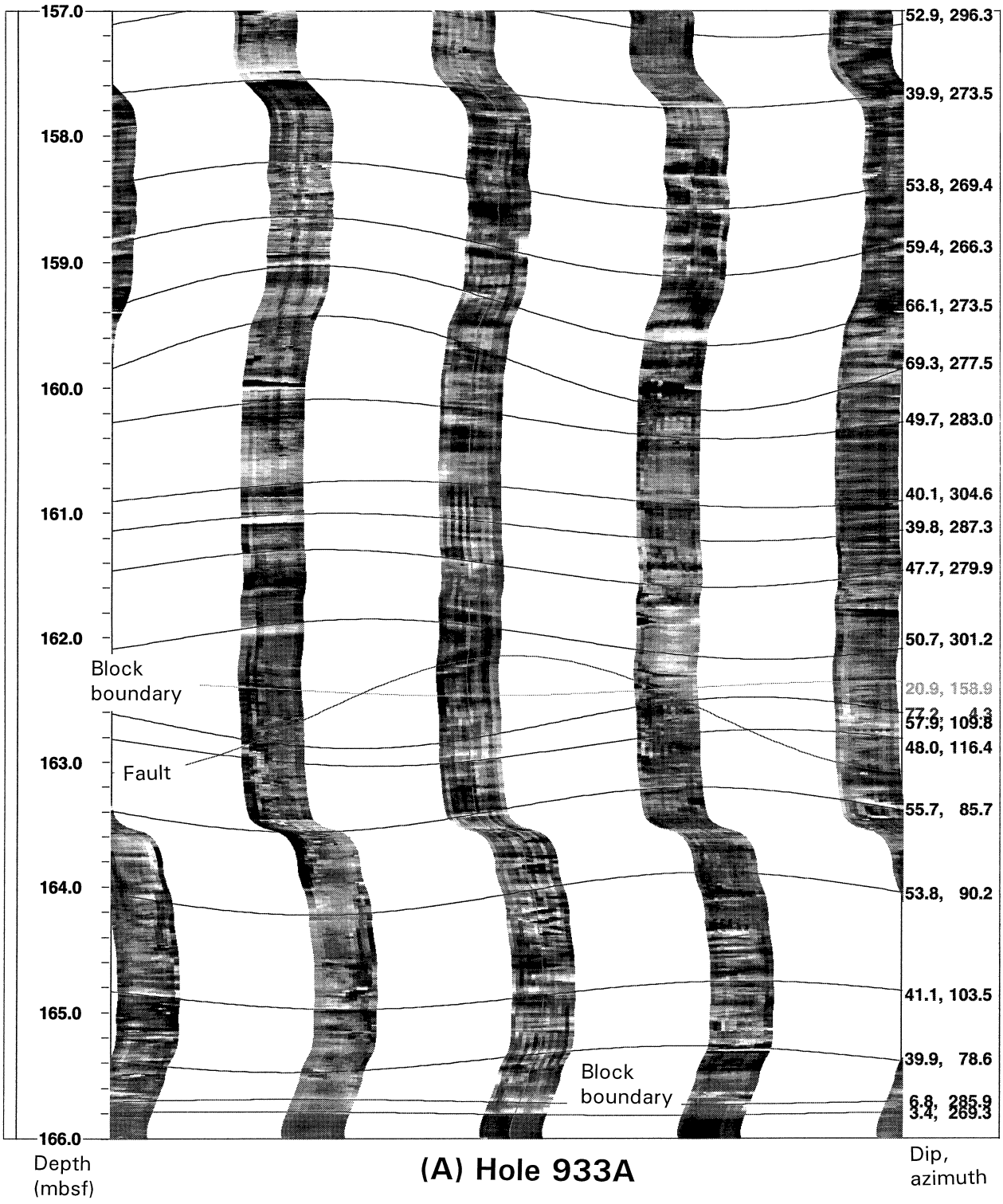

Figure 16. Examples of particular features from Formation MicroScanner logs. In all plots, thin wavy lines indicate bedding surfaces that can be correlated between pads. Numbers on right are dips and azimuths determined from these bedding surfaces. **A.** Hole 933A, 157–166 mbsf. Note 180° change in azimuth across fault or block boundary.

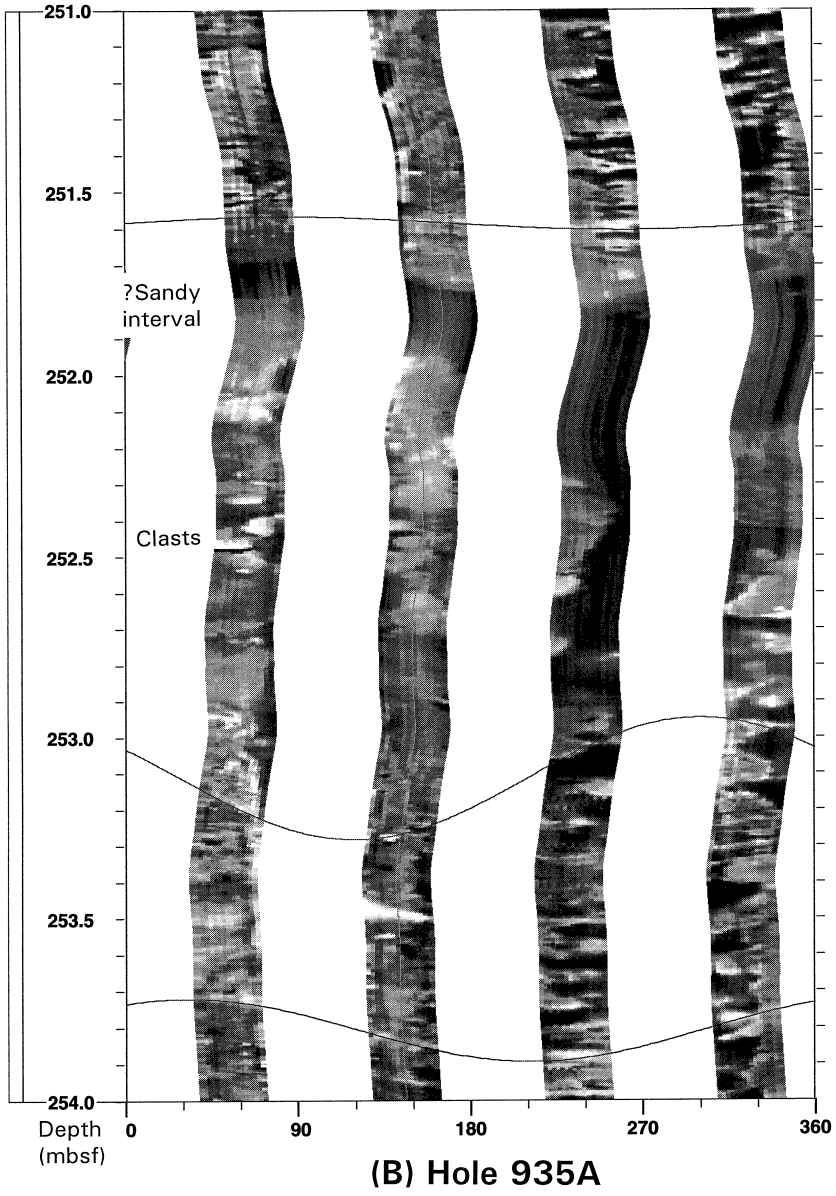

Figure 16 (continued). **B.** Hole 935A, 251–254 mbsf, showing abundant clasts and sandy interval.

dip and azimuth tend to group with a more or less constant value. We interpret these zones to represent blocks that moved in a coherent fashion within the MTD. Further analysis is needed at this point to determine the axis of folds and the exact nature of faults within the unit. The apparent block boundaries occur at intervals ranging from a few meters up to ≈20 m. At Hole 933A, the "block" dimensions appear to decrease uphole, but no such trend is visible at Sites 936 and 944.

A summary plot of the azimuth of the measured features within the MTDs for each hole is presented in map view in Figure 22. At Site 933, most beds dip to the west-southwest with secondary modes to the southeast and to the east. This corresponds to the apparent dip of the Bottom Levee Complex levee at Site 933 as seen in a seismic-reflection profile crossing the site (Flood, Piper, Klaus, et al., 1995, "Site 933" chapter, fig. 2). Sites 935, 936, and 944 display the majority of beds dipping to the south-southwest, southeast and east-southeast, respectively. At Sites 935 and 936 the overall azimuth of the bed-dips is opposite to the surface downslope direction. At Sites 936 and 944, the URMTD overlies the western flank of the Red Channel-levee System and the azimuth of dipping beds corresponds to the apparent dip of the Middle Levee Complex at these locations. The dips determined from seismic-reflection profiles are to the east at Site 936, consistent with the true dip direction observed from the FMS data at this site. Site 935 is located south of the Gold-Green bifurcation, a prominent topographic high, and the azimuth of dip for the MTD corresponds to the bottom topography at the time it was emplaced.

Some observations of deformation can be made in split core face. Matrix material (m in Fig. 15E) lacks internal stratification, but may contain streaked blebs of different color or grain size. Many individual blocks show shearing (Fig. 18E) and folding (Fig. 18F), but are also offset by brittle faults (Fig. 18F). There may be a continuum between deformed less consolidated blocks and true matrix in taking up shear within the MTD. Brittle faulting may in part develop during post-depositional consolidation.

Lithologic Properties of Clasts

Grain-size data presented by Manley et al. (this volume) show that most clasts are relatively clay-rich sediments, comparable with upper fan levees. In general, samples are finer grained than the immediately

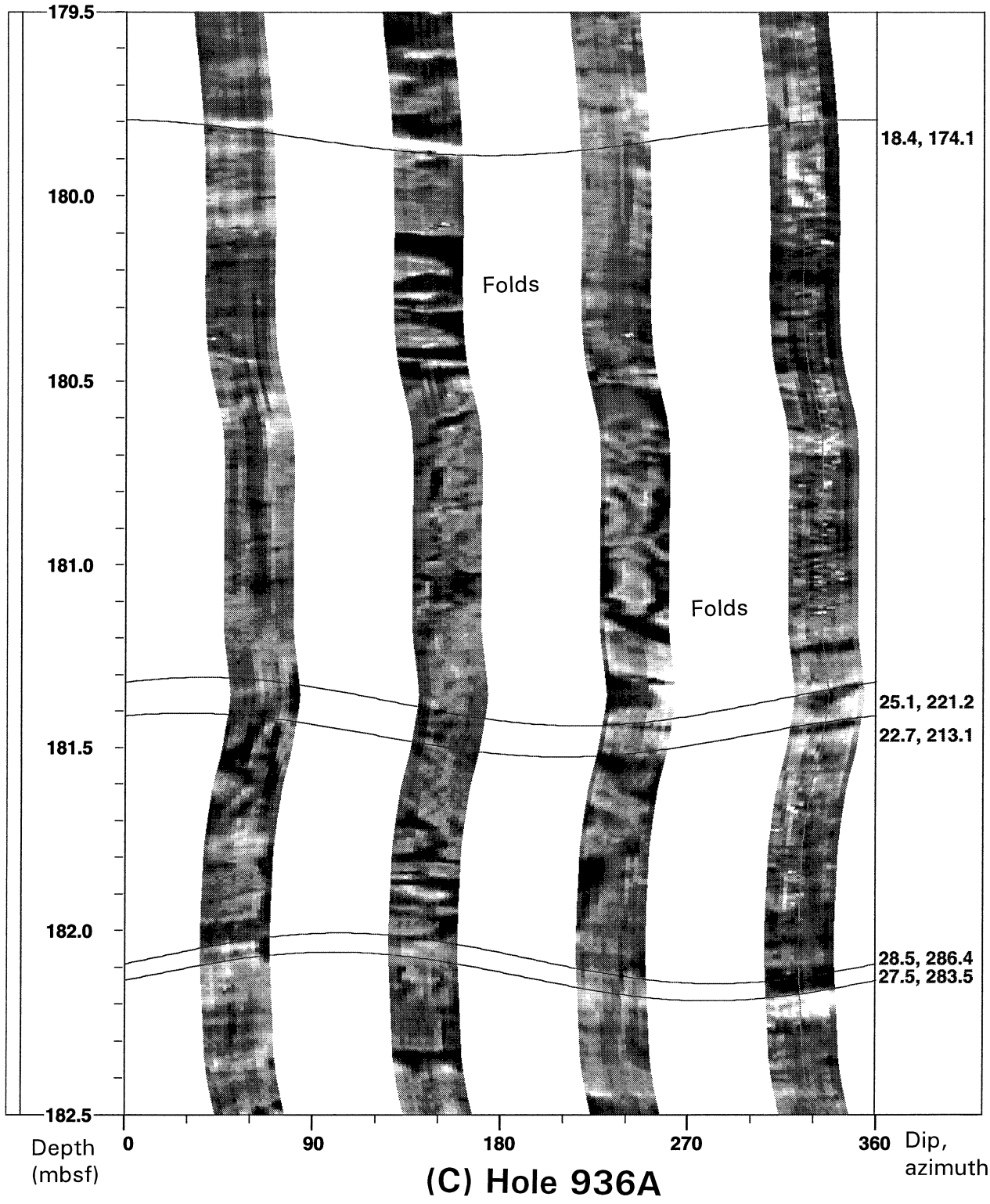

Figure 16 (continued). **C.** Hole 936A, 179.5–182.5 mbsf, showing small-scale folding.

underlying levees. However, some samples are indistinguishable in their grain size from local levee sediments.

The FMS images within the MTDs display a variety of electric facies (see Pirmez et al., this volume), but are generally dominated by thinly laminated units (Fig. 16D). Thin resistive layers observed on the images probably correspond to silt and silty-sand intervals noted in many cores of URMTD (e.g., Fig. 15B). The resistive layers provide good markers that can be traced between pads for measuring dips Locally thicker resistive beds are observed on the FMS images, often contained within the image of a single pad, and are interpreted as sandier intervals. The overall characteristics of the FMS images within the URMTD suggest that the electric facies of many of the

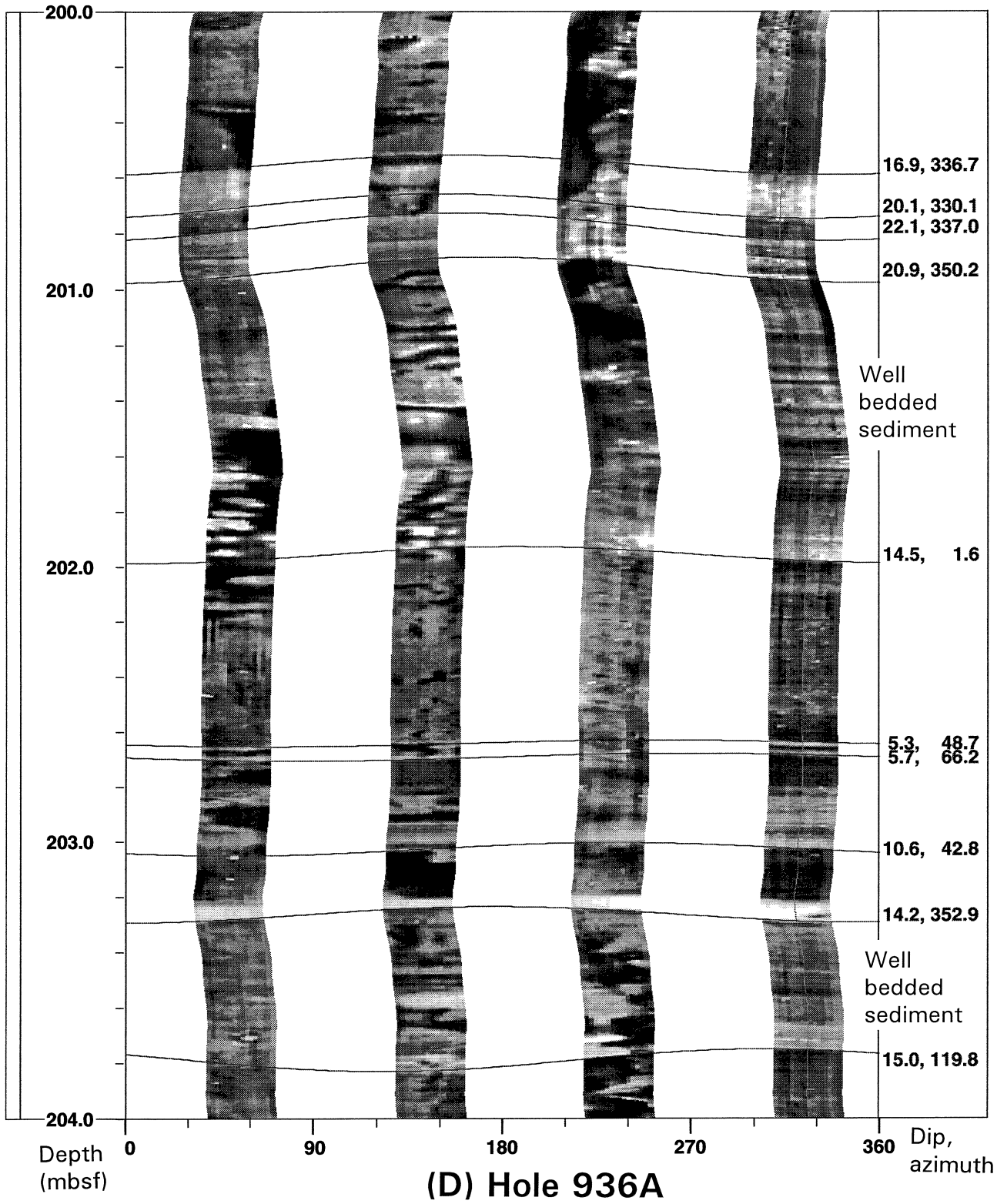

Figure 16 (continued). **D.** Hole 936A, 200–204 mbsf showing well-bedded silts and muds resembling those found in levee sequences.

blocks is quite similar to channel-levee deposits examined on Amazon Fan. The images display typical characteristics of turbidite beds, such as grading (decreasing resistivity upward) and erosional bases where thicker, resistive beds occur.

Sediments in the MTDs in general contain a higher proportion of benthic foraminifers than do the autochthonous levee muds cored at the same site (see tables of foraminiferal data for individual sites in Flood, Piper, Klaus, et al., 1995). Many of the benthic foraminifers appear to be mid- to upper bathyal, with rare outer shelf taxa (Vilela and Maslin, this volume). Many MTDs contain echinoid spines. Bioturbation by echinoids was recognized only at shallower water sites such as 937, 938, and 942. Clasts of interglacial calcareous clay,

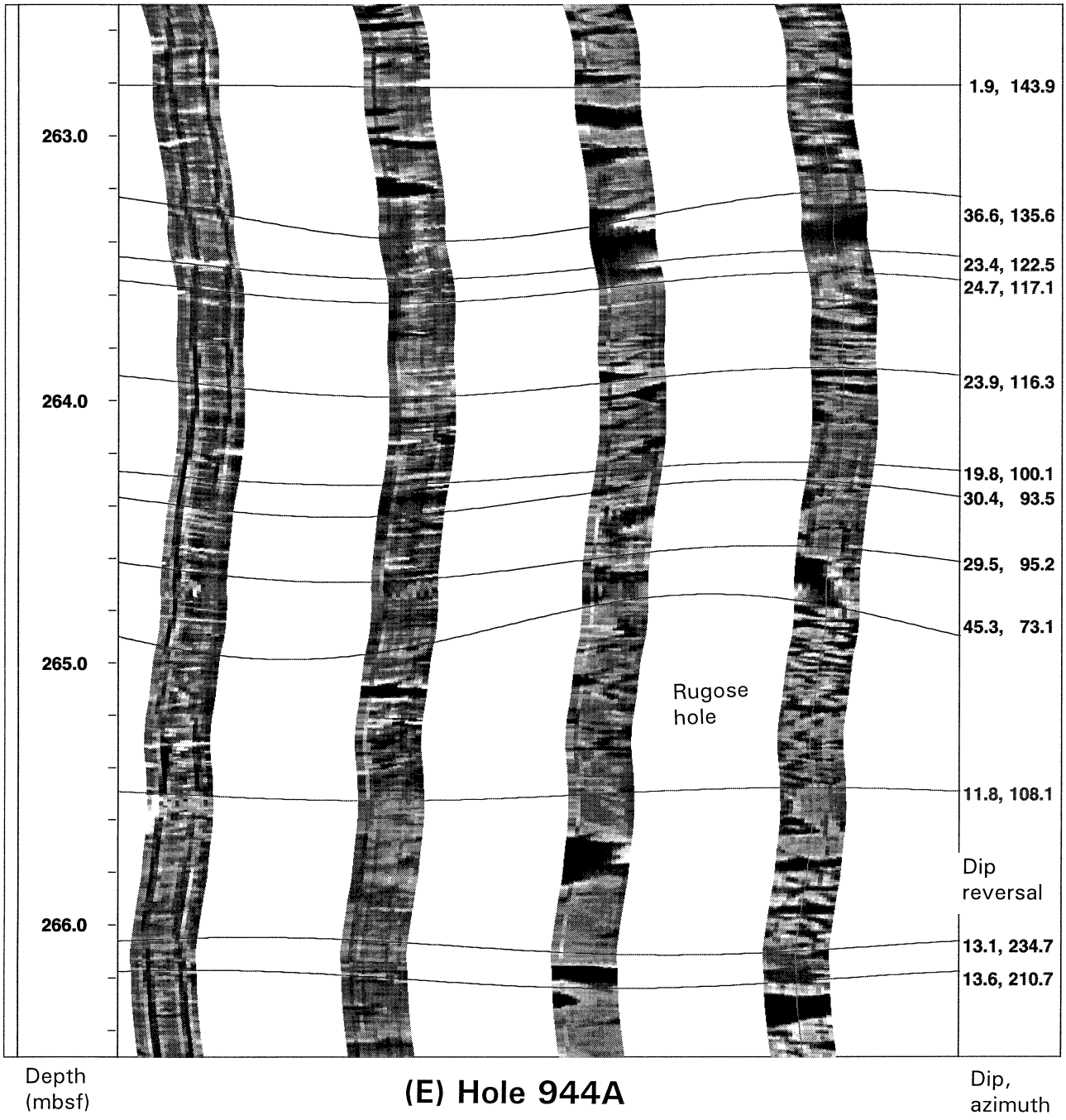

Figure 16 (continued). **E.** Hole 944A, 263–266 mbsf showing abrupt contacts and changes in azimuth between blocks.

wherever recovered during Leg 155, are particularly distinctive because of their light color. Many of these calcareous clays lack bathyal benthic foraminifers and are therefore unlikely to have been transported from the continental slope.

At several sites, a few microfossil samples are barren of bathyal benthic foraminifers and contain rare abyssal benthic foraminifers (Samples 155-935A-25X-5, 59–64 cm, and 27X-CC; 155-944A-26X-CC and 28X-CC). These blocks presumably originated in abyssal water depths.

Clay minerals are not generally diagnostic of source, but the lower part of the MTD at Site 931 has a distinctive chlorite that is only found in the levee sediment from the Bottom Levee Complex during this leg. This supports the lithologic observation of the unusual occurrence of small-scale blocks at the base of the deposit, suggesting that local erosion may have occurred.

Evidence for Gas Hydrates

Unequivocal evidence is lacking for gas hydrates in sediment recovered during Leg 155. Extremely gassy sediment was recovered from the WMTD at Site 941 that is associated with low-chlorinity pore water, interpreted as evidence of gas hydrates by Soh (this volume). Shipboard chlorinity measurements were made at infrequent intervals: anomalously low values are found in MTDs at Sites 941 (<500 mM), 936 (547 mM), and 933 (549 mM), but not at other sites. (Low chlorinity occurs in permeable HARPs at Sites 931 and 935.)

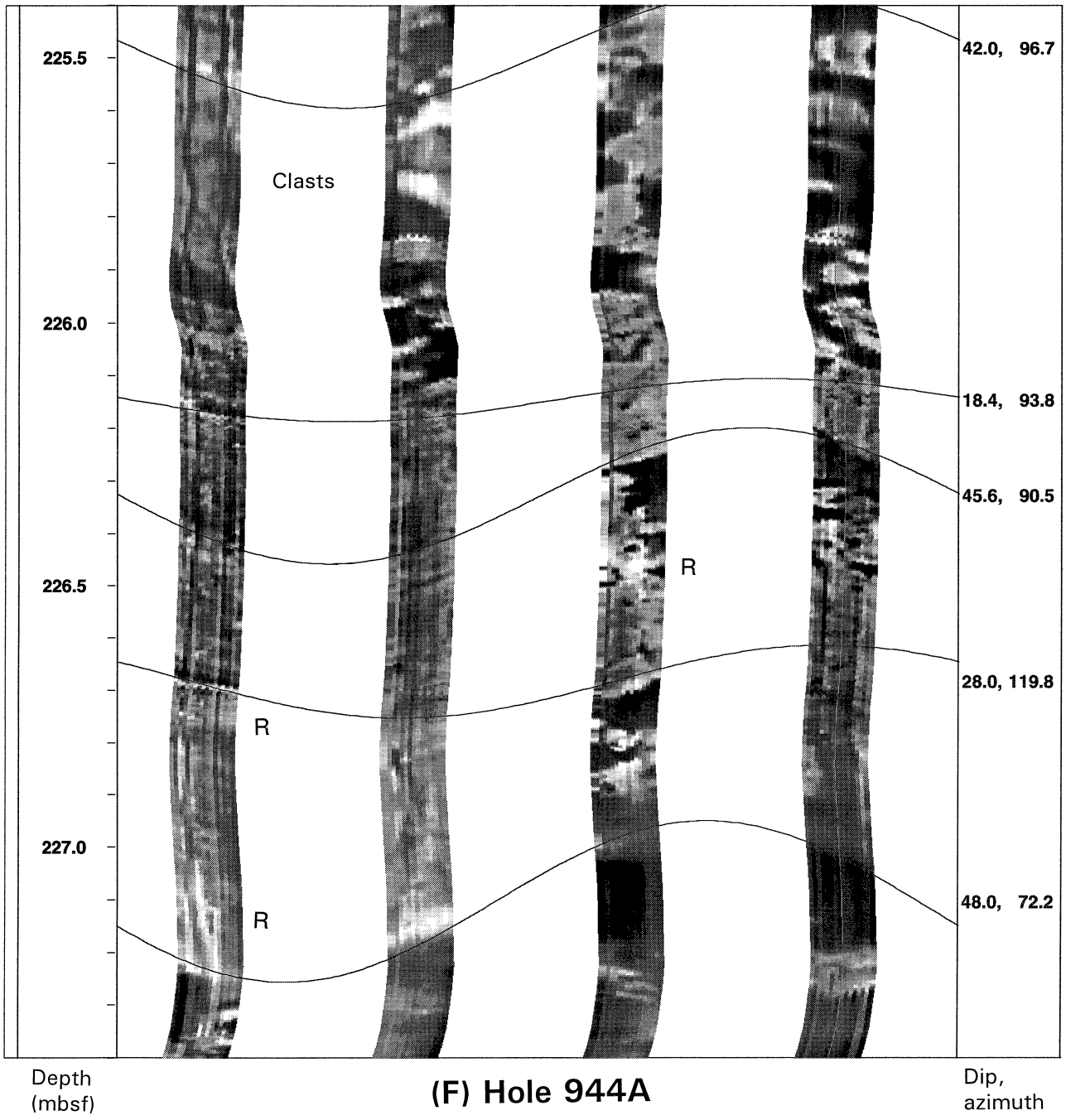

Figure 16 (continued). **F.** Hole 944A, 225.5–227.5 mbsf, showing abundant clasts. R = resistive clast (?hard clay).

Correlation Between Holes

In places, it seems possible to correlate specific features between nearby holes. At Site 941, correlation of cyclical variations in foraminiferal assemblages and water content appears to be possible between the A and B holes, which are 500 m apart (Fig. 17). Magnetic susceptibility in the BMTD changes abruptly at 275 mbsf in Site 931 and 125 mbsf in Site 933 (Table 2; Fig. 14), but other parameters (such as total nitrogen) do not correlate.

Sites 935 and 936 both have long intervals of uniform mud in the lower part of the URMTD, suggesting that large blocks are present. In detail, however, the blocks are quite different at the two sites. Unit C at Site 935 (Fig. 14) has abundant *P. obliquiloculata* and *Globigerinoides ruber* and sparse bathyal benthic foraminifers; in contrast, the lower part of URMTD at Site 936 has abundant bathyal benthic foraminifers but *P. obliquiloculata* and *G. ruber* are rare (Table 2). The basal part of URMTD at Site 944 is similar to that at Site 936 in lithology and many microfossil properties.

Manley et al. (this volume) suggest that there is a significant downfan increase in modal size within the URMTD, from ~7.2ϕ at Sites 935 and 936 to 5.8ϕ at Site 944. This change seems to represent higher percentages of sand (5%–20%; cf. 1%–5% upfan) at Site 944 and parallels a similar increase in autochthonous sediment.

Similarities in the sequence of lithologies between Sites 931, 933, and 935 support the suggestion from seismic-reflection data that the BMTD and URMTD may be correlative. Unit A at Sites 931 and 935

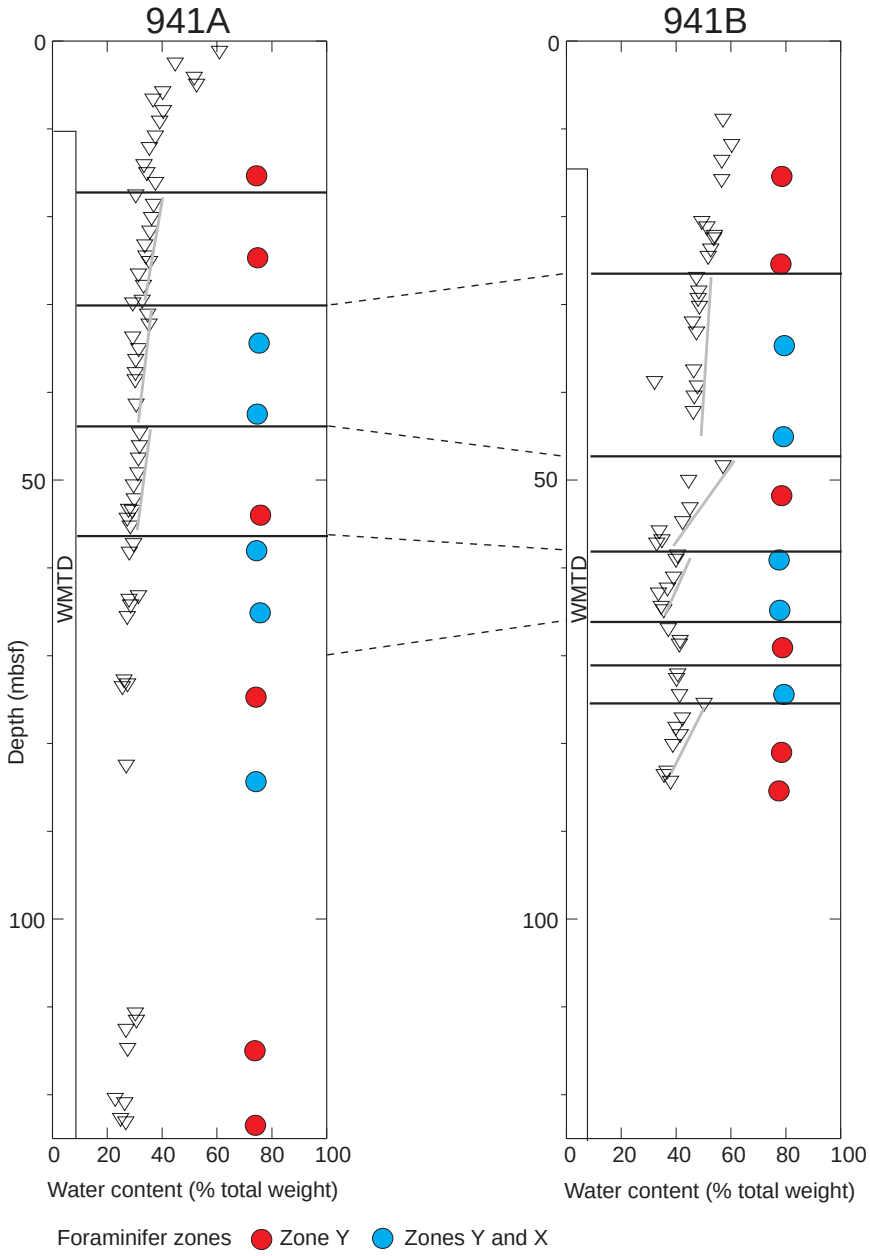

Figure 17. Downcore variation in water content and foraminiferal assemblages in WMTD at Site 941 supporting interpretation of large, discrete blocks. (Data from "Site 941" chapter in Flood, Piper, Klaus, et al. 1995). Zone Y is glacial, Zone X interglacial.

(Fig. 14) has similar folded muds with silt laminae, common *P. obliquiloculata*, but sparse *G. ruber*. Unit D in Site 931, B in Site 933 and C in Site 935 (Fig. 14) are all lithologically uniform, have abundant *P. obliquiloculata* and *G. ruber*, rare benthic foraminifers, and similar magnetic susceptibility. The upper part of Unit B at Site 936 (to ~205 mbsf) appears lithologically and micropaleontologically similar, although block size is somewhat smaller than at Site 935. The lower half of URMTD at Site 936 resembles that at Site 944 (Fig. 14; Table 2), thus suggesting that the URMTD at Site 936 may be composite (see "Discussion" section).

PHYSICAL PROPERTIES

Introduction

In this section, we examine results from post-cruise studies of physical properties. Much of the basic data for this study is presented in individual site chapters of Flood, Piper, Klaus, et al. (1995). In particular, we discuss data concerning the strength properties of sediment in the MTDs.

Western Mass-Transport Deposit

In the WMTD, careful observation of the split core face allowed distinction of matrix and clasts in some sections (e.g., Fig. 15E). Closely spaced torvane measurements illustrate significant differences in undrained shear strength (*Su*) of clasts and matrix. A clast at 155-941A-4H-4, 105 cm, has *Su* = 95.9 kPa, whereas nearby matrix at 941A-4H-4, 109 cm, has *Su* = 30.3 kPa. Matrix samples are remolded and effectively underconsolidated (these particular samples have ~30 m of overburden), because of the rapid emplacement. The shear strength of the clasts, which are normally to overconsolidated, result from loading to higher stress levels at their former site. Based on the undrained shear strength profiles of the shallowest Leg 155 sites (i.e., Sites 937, 938, and 939: Flood, Piper, Klaus, et al., 1995), the clast would have been derived from sediment buried to at least

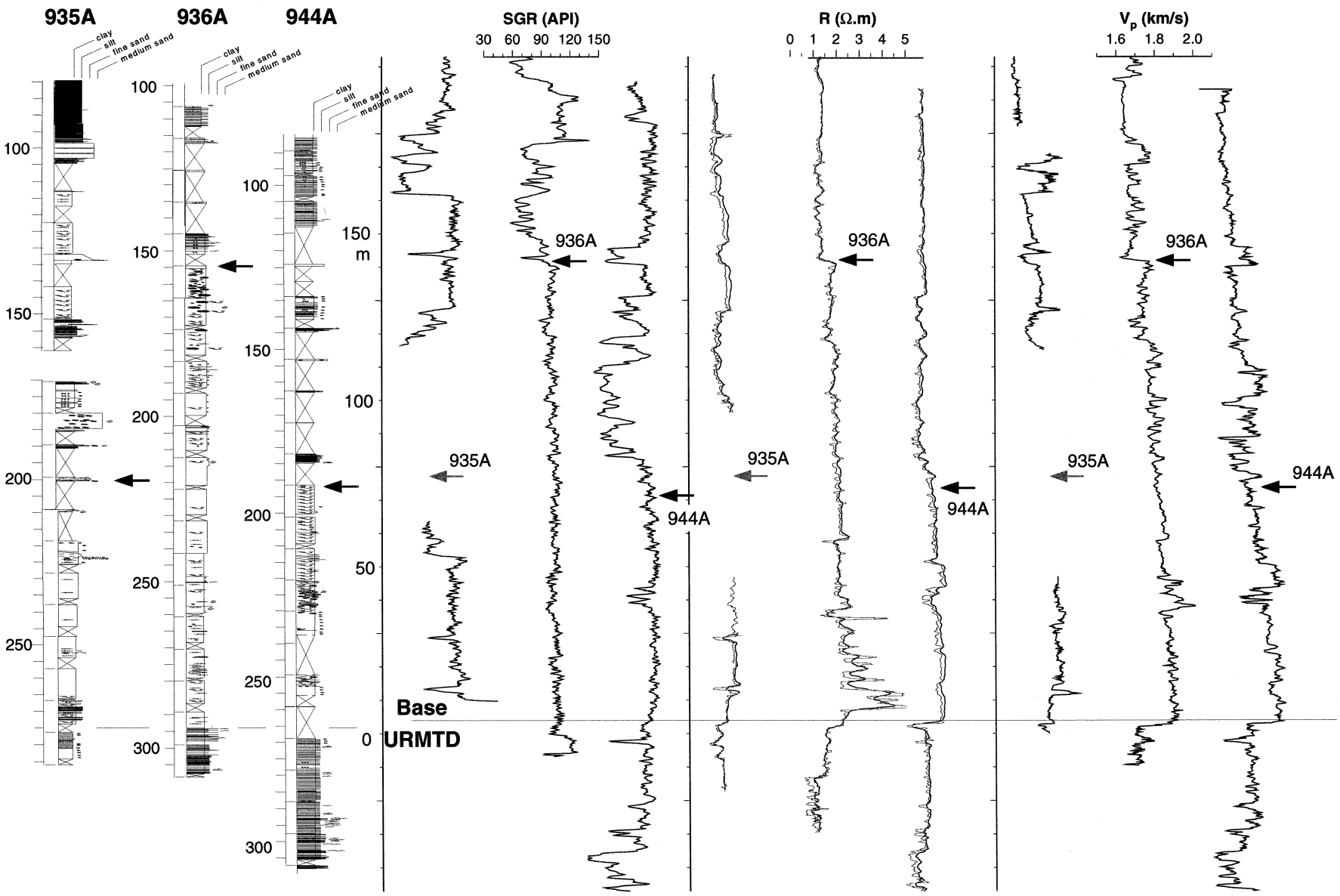

Figure 18. Wireline logs of the URMTD at Sites 935, 936, and 944. Each site is aligned to the base of the URMTD; top of URMTD is indicated by bold arrow.

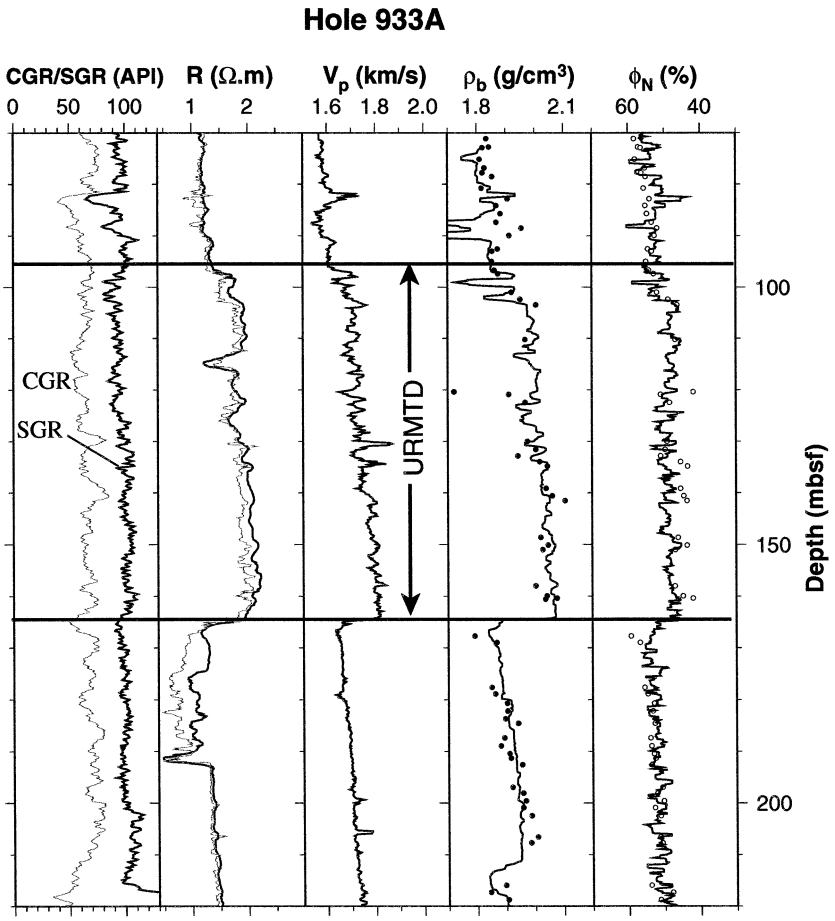

Figure 19. Wireline logs of the BMTD at Site 933.

100 mbsf if it was late Pleistocene sediment with a similar consolidation history or it could have been derived from a shallower depth if it was older material. The clast measured at 155-941A-4H-4, 105 cm, is relatively the firmest; other clasts have lower strengths suggesting that a wide range of source material is incorporated within the MTD. Both the matrix and the clasts must support the present overburden stresses. In the clasts, all the overburden is carried by effective or intergranular stress. In the matrix, some overburden is carried by effective or intergranular stress and some could be carried by excess porewater pressure.

Consolidation testing was carried out on four samples from the WMTD at Site 941 (Fig. 23) and one sample from the underlying levee deposit. All consolidation test results suggest that disturbance had occurred, as the C_c/LL (compression index/liquid limit) ratio is close to that of remolded material (Terzaghi and Peck, 1967). It is not clear from adjacent sediment what the proportion of blocks to matrix is in the samples, although the two deepest samples from the WMTD probably consist of decimeter-sized blocks separated by matrix. The upper three samples from the WMTD yielded similar preconsolidation values (39.1, 57.1, and 65.9 mbsf, Pc' values 167, 175, and 177 kPa, respectively), suggesting a similar stress history: these three tests may represent the behavior of matrix material that supports the more compacted blocks. A deeper sample at 72.33 mbsf had a Pc' of 400 kPa, which is higher than that determined in a consolidation test of deeper levee sediment underlying the MTD (Pc' of 305 kPa at 163.05 mbsf). The lowest mass-transport sample at 72.33 mbsf probably represents the stress history of a single block.

At Site 941, the MTD has undrained shear strength/effective overburden stress ratios (Su/Po') generally at least double that of the underlying levee sediments. Po' is calculated from the measured bulk density values integrated over the overburden depth interval and used as buoyant densities (Moran et al., 1993). The ratio in the MTD of ~0.1 is below that of normal consolidation (Skempton, 1970), which should be ~0.2 to 0.3., but is similar to that of the other Leg 155 sites. The profile shows a wide scatter of values (Fig. 24). Some scatter may be the result of drilling disturbance, but it is principally due to the testing of both matrix and blocks that have quite different stress histories.

On the basis of Skempton's (1970) approximation, and assuming full consolidation of sediments is possible, the low Su/Po' ratio would indicate that the sediments are underconsolidated. Gibson (1958) showed that for a clay to be normally consolidated with a uniform rate of deposition (r), the ratio c_v/rh must be more than 10 where h is the thickness of the layer and c_v is the coefficient of consolidation. Results of consolidation testing indicate the latter is typically 1 m^2/year, so then for the top 100 m the deposition rate has to be less than 1 m/k.y. The initial results from Leg 155 (Flood, Piper, Klaus, et al., 1995, see "Leg Synthesis") indicate that this rate of deposition was frequently exceeded. Therefore, it is not surprising that the sediments recovered indicate underconsolidation. The presence of free gas or hydrates would also inhibit the normal consolidation processes.

Bottom Mass-Transport Deposit

The MTD at Site 931 has undrained shear strength/effective overburden stress ratios (Su/Po') of ~0.07, generally at least half that of the overlying sediments (Fig. 25). Such ratios are minimum values due to the limits of the shipboard measuring equipment (Flood, Piper, Klaus, et al., 1995, see "Explanatory Notes"). The scatter in Su/Po'

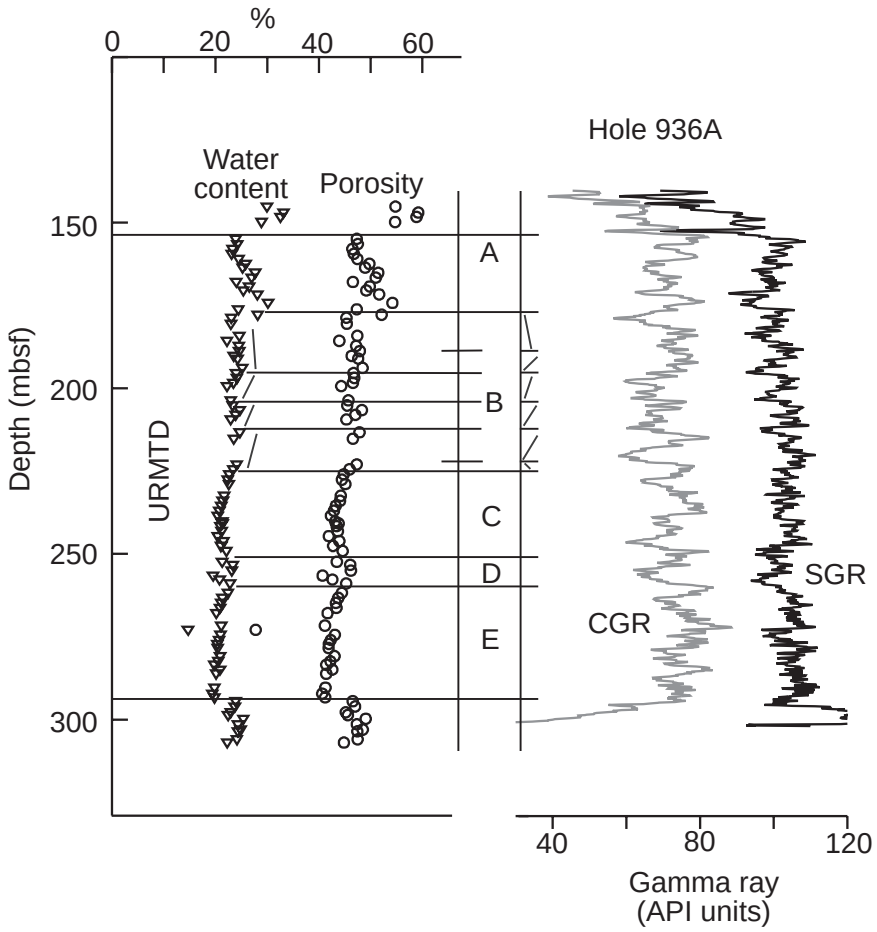

Figure 20. Selected index and wireline log properties in URMTD at Site 936, supporting interpretation of large, discrete blocks.

between 0.02 and 0.08 may in part be due to core disturbance, but, as at Site 941, probably represents the non-uniform distribution of clasts within the matrix.

The BMTD at Site 931 can be divided into three subunits on the basis of shipboard measured index properties (Figs. 25, 26) and shear strength (Flood, Piper, Klaus, et al., 1995). The stiffest sediment is found in the lowest part of the deposit (297–348 mbsf) where undrained compressive strengths are >440 kPa and undrained shear strength was measured as 320 kPa by a single laboratory vane measurement. All other laboratory vane tests exceeded the machine capability. Such high strength values suggest that the BMTD was derived from old, stiff sediment. Sediment of this consolidation state is unlikely to occur within 100 mbsf on the Amazon Fan (based on Leg 155 results). A source area on the continental slope or shelf is considered more likely from the degree of consolidation.

The index properties at Site 933 clearly show the effect of restricted dewatering of the sediment immediately underlying the MTD (Fig. 27). The water-content profile of the sediment immediately below the BMTD follows the same trend as the sediments overlying the MTD (Fig. 28). The single exception is the sample (155-933A-19X-1, 51–53 cm) just below the MTD (Fig. 28), where trends in log data (Fig. 19), particularly resistivity, have been interpreted as indicating considerable overpressure (Flood, Piper, Klaus, et al., 1995), suggesting that the BMTD has inhibited drainage. These observations suggest that there was no major erosion at the base of the BMTD during its emplacement.

The index properties at Site 933 also show evidence for discontinuities in physical properties of blocks in the BMTD, with a major boundary at 133 mbsf (Fig. 27). Both above and below this boundary, the water content gradually increases with depth (*sic*). The FMS data suggest that most of the index property measurements were made in clasts, implying that progressively more consolidated material was incorporated into the MTD and accumulated higher in the deposit (or perhaps that more matrix is present deeper in the section). The higher undrained shear strength values at the top of the lower subunit would support this interpretation. The upper sequence (above 133 mbsf) generally has higher water contents and may be derived from younger less consolidated sediments.

Flood et al. (this volume) have shown that shear modulus and bulk modulus determinations (based on analysis of porosity and log-derived velocity) indicate normal to overconsolidated sediment immediately below the BMTD at Site 933 and underconsolidated sediment beneath the URMTD at Sites 936 and 944. This interpretation at Site 933 is inconsistent with the interpretation of an underconsolidated unit beneath the BMTD at this site based on water content and resistivity log data.

AGE

Introduction

Aboard ship, the age of buried MTDs was poorly constrained and several of the deposits appeared to mark major hiatuses in sedimentation. For example, the BMTD overlies mid-Pleistocene (probably isotopic Stage 7) calcareous clays and is overlain by late Pleistocene deposits of Channels “5” and “6” (Fig. 3), dating from isotopic Stage 3 (Maslin and Mikkelsen, this volume). Determining whether the MTDs have removed sediment by erosion or are overlain by hiatuses

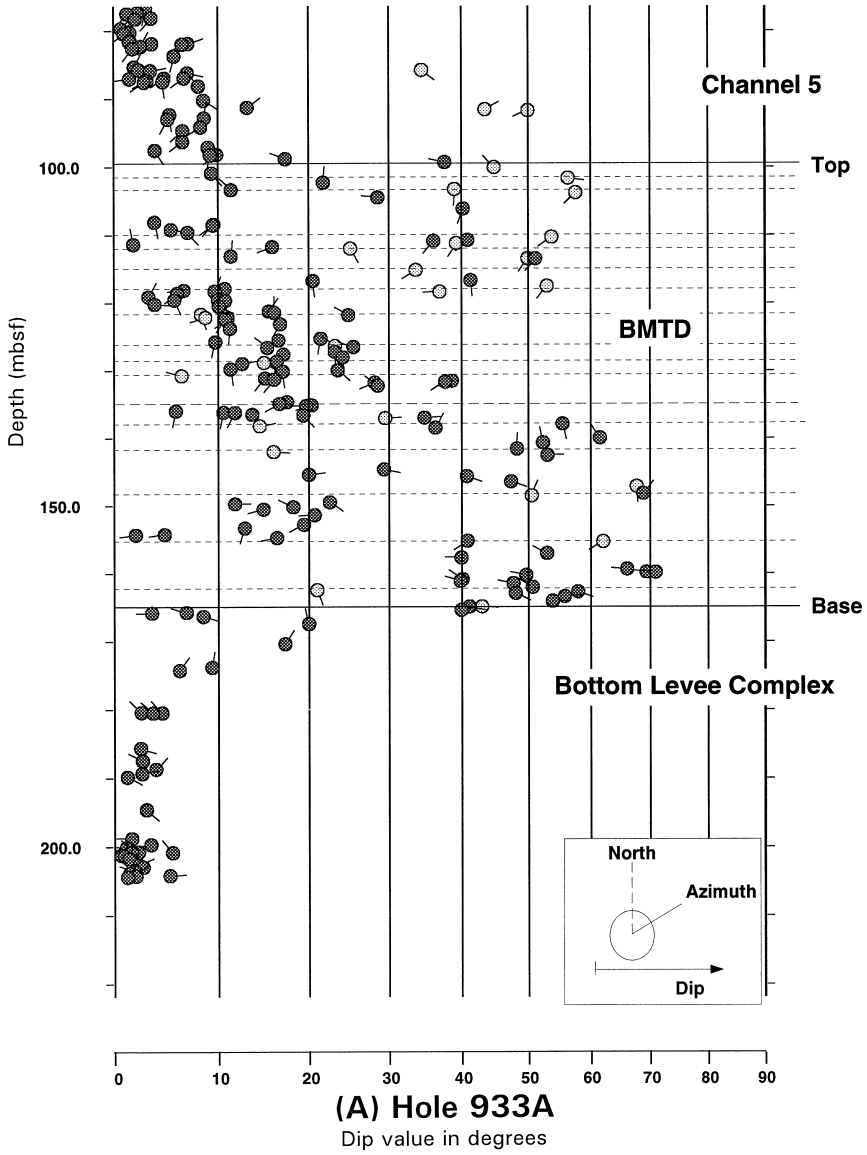

Figure 21. Dip-azimuth ("tadpole") plots for MTDs in (**A**) Hole 933A, (**B**) Hole 936A, and (**C**) Hole 944A. Also shown is (**D**) an azimuth vs. depth plot for Hole 933A. Thin dashed lines mark the apparent block boundaries where azimuth and or dip change rapidly within the hole. The vertical gray bars in (D) mark the vertical extent and the average azimuth of beds measured.

is important in determining the origin and nature of their emplacement. Surficial debris flows, such as the WMTD, provide more accessible examples for considering the possible presence of hiatuses overlying debris flows.

Western Mass-Transport Deposit

Damuth and Embley (1981) obtained 50 cm of Holocene calcareous ooze over 435 cm of gray clay resting on debris flow deposits in core V18-20. Using a sedimentation rate of 0.5–1.0 m/k.y. for the late glacial gray clay, they estimated an age of 15–25 ka for the base of the sediment overlying the WMTD. Rates of sedimentation for muddy sequences on Leg 155 (e.g., at Site 932) are >1 m/k.y., suggesting the younger end of this range is more probable. Oxygen isotope determinations from this core V18-20 (Fig. 29) show values of $\delta^{18}O$ on *Globigerinoides sacculifer* just above the MTD of ~0.0, similar to those just above the last glacial maximum in Site 942. The bottom of core V12-88, which did not reach the MTD, appears to be younger.

A younger age (early Holocene) was estimated for the WMTD at Site 941 during Leg 155 (Flood, Piper, Klaus, et al., 1995). The interpretation of the age of the WMTD is critically dependent on identifying the top of the deposit at Site 941. The following lithologic units were distinguished in Hole 941A (Flood, Piper, Klaus, et al., 1995). Unit I (0 to 0.98 mbsf) consists of brown calcareous clay. Unit II (0.9 to 8–5.3 mbsf) consists of mottled gray clay. Unit III, consisting principally of mud clast conglomerate and large mud blocks, was identified as the MTD. However, the uppermost part of Unit III (to 10.7 mbsf—155-941A-2H-5, 64 cm) also consists of mottled gray clay similar to that in Unit II. This interval contains abundant branching siliceous fossils (3 mm × 10 mm). Three clasts, a few centimeters in size, occur in the mottled mud of Unit III. This mud has an abrupt contact with an underlying mud-clast conglomerate. This upper 5 m of Unit III might represent in situ sedimentation involving winnowing off the top of the blocky MTD (and rare spalling of clasts), or might represent a debris flow deposit forming the upper part of the mass-transport unit. The presence of siliceous branching fossils and of mottling (bioturbation) throughout suggests that it represents relatively slow autochthonous (hemipelagic) sedimentation. This interpretation is supported by the very consistent isotopic character of *G. sacculifer* in three samples from this mud interval with $\delta^{18}O$ of 0.2‰–0.3‰, identical to values at the last glacial maximum peak in nearby Site 942 (Showers et al., this volume). Samples elsewhere in Unit III show more variability, consistent with an interpretation of mixed sources, so it is difficult to explain the consistent isotopic signature

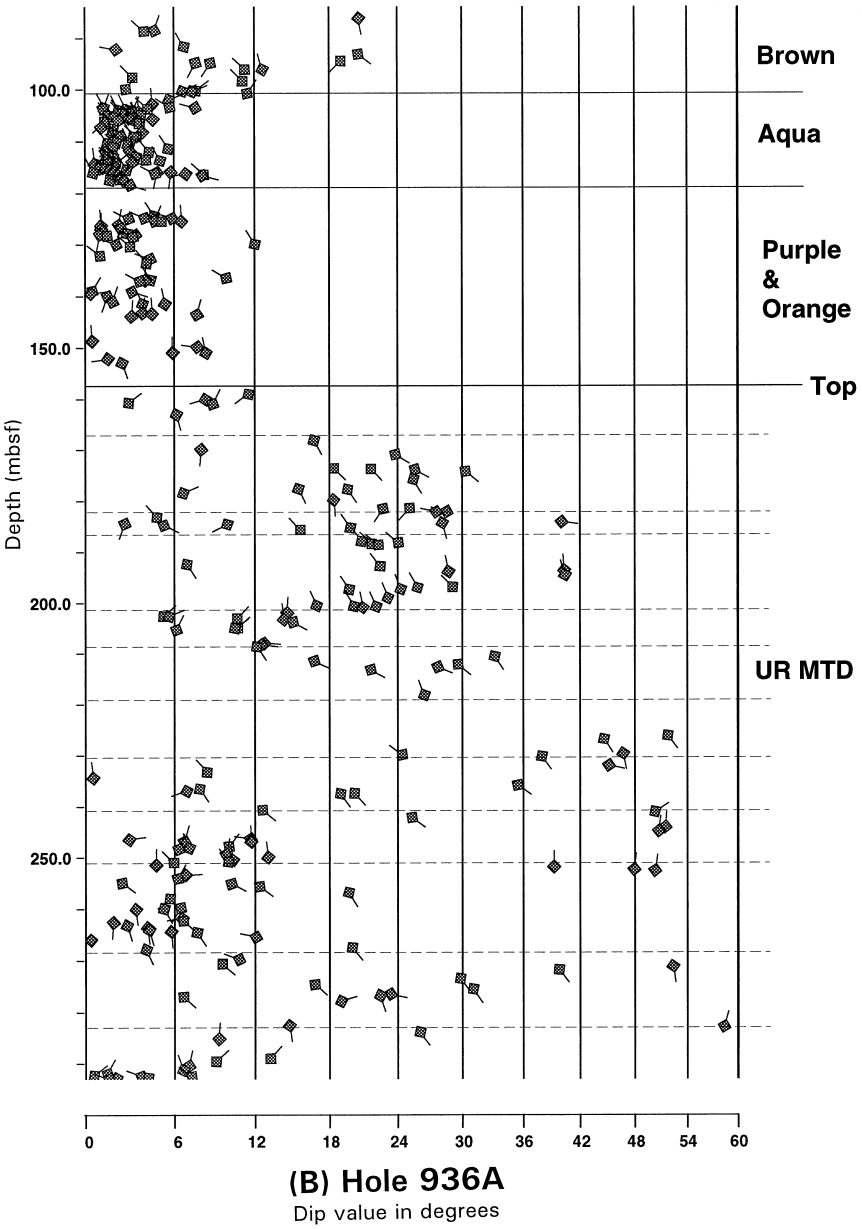

Figure 21 (continued).

of the mottled mud interval at the top of Unit III if it is a debris flow deposit. If the interpretation of autochthonous sedimentation is correct, the base of the sediment overlying the WMTD corresponds approximately to the last glacial maximum in isotopic Stage 2.

It is possible that cores penetrating to the WMTD were located on high-standing blocks in the deposit and thus have a significant local hiatus, as sediment first filled depressions between blocks. In this case, the age of the oldest overlying sediment may not be an estimator for the age of the MTD. At Site 941, blocks have ~5 m of relief, although 15-m blocks are seen nearby in 3.5-kHz profiles. Sedimentation rates on abandoned high-standing levees, such as at Site 932, are ~1.1 m/k.y., so it is possible that a hiatus of several thousand years may be present on the top of blocks in the MTDs.

Seismic-reflection profiles suggest correlation of the snout of the WMTD (Flood, Piper, Klaus, et al., 1995, "Site 941" chapter, fig. 4) with the lower part of the Amazon-Brown interval, but this correlation remains tentative. Sediment underlying the WMTD is tentatively correlated through the seismic stratigraphy with the Purple Channel-levee System, consistent with the lack of *P. obliquiloculata* (which is absent between ~40 and 10 ka; Maslin et al., this volume). The range of isotopic data is similar to that from the Purple interval at Hole 930B and 937B (Showers et al., this volume). The age of the Purple interval is estimated to be ~22 ka (Piper et al., this volume). The thickness of the "missing" stratigraphic section between the autochthonous sediments above and below the WMTD can be estimated. Six meters of non-recovery separates the base of the MTD and the top of the Purple levee. If the top of the MTD immediately predates Stage 2.2 (18 ka, corresponding to the Brown Channel-levee System) then only a short time interval, equivalent to the Aqua Channel-levee System of perhaps 4 k.y. duration, is not represented at the site (Piper et al., this volume). Site 941 is near the downslope limit of the WMTD: greater erosion may have occurred upslope.

Other Surficial Mass-Transport Deposits

The age of the EMTD can only be estimated from piston cores, because it was not drilled during Leg 155. Oxygen isotope analyses on RC16-171 (Fig. 29) suggests that the top of the core is missing and

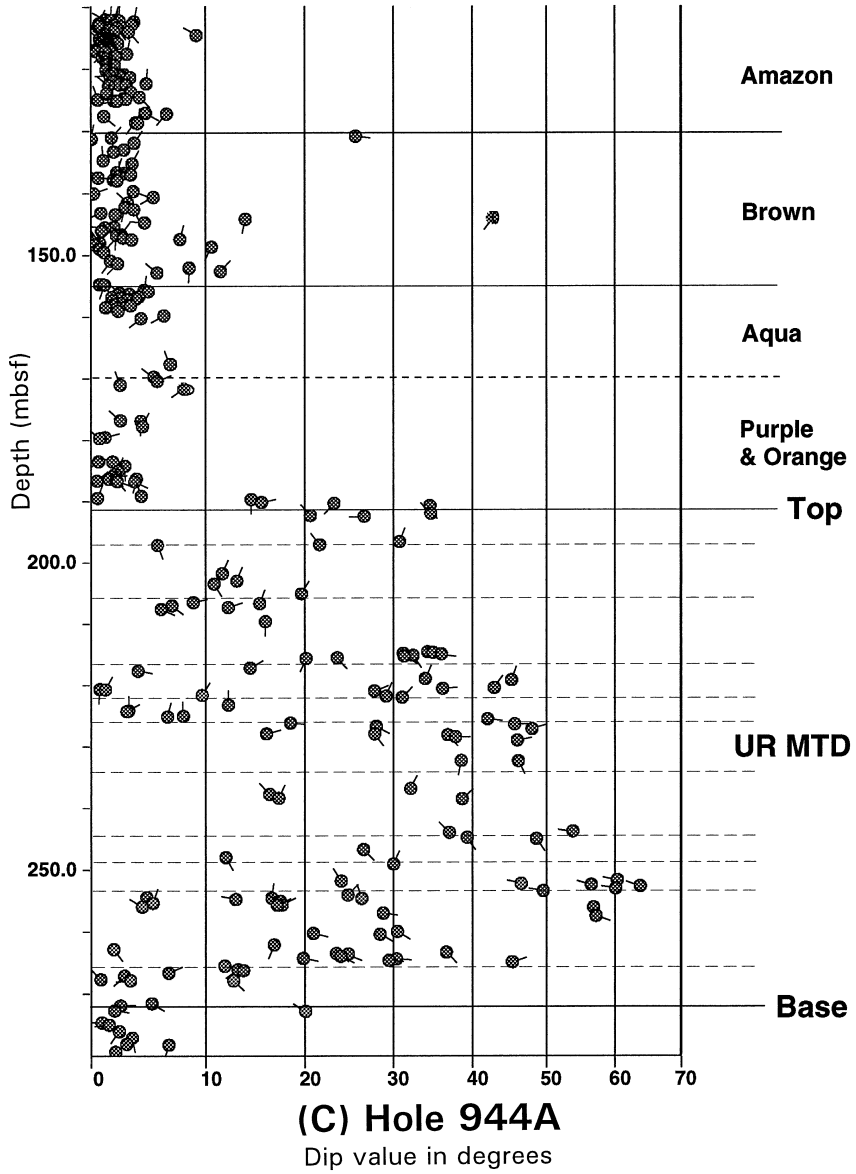

Figure 21 (continued).

that Stage 3 sediment is present above the MTD. Alternatively, the sediment may be mixed, including dominantly isotopically heavy glacial age foraminifers and a few Holocene individuals (because *G. menardii* is reported to 5 mbsf).

A similar isotopic stratigraphy was obtained from RC15-176 on the MTD near 50°W, where the MTD underlies Stage 3.3. On the other hand, core V31-139 on the eastern part of the same MTD has an isotopic stratigraphy similar to that found on the WMTD, supporting the interpretation of Damuth and Embley (1981) that this MTD may be composite.

Unit R Mass-Transport Deposit

Regional seismic-stratigraphic correlation shows that the URMTD overlies the Red Channel-levee System of the Middle Levee Complex (Figs. 2, 3, 11), dated as older than isotopic Stage 5 by seismic correlation with Site 942 and younger than Stage 7 at Sites 936 and 944. The lowest HARP above the URMTD in Site 935 is correlated through seismic profiles with the Orange Channel-levee System (Fig. 3), dated at Site 930 at ~40 ka based on the appearance of *P. obliquiloculata* (cf. Maslin et al., this volume).

At Site 935, the *P. obliquiloculata* datum occurs in hemipelagic mud overlying a HARP that rests on the mass transport unit (Fig. 3). At Site 936, the *P. obliquiloculata* datum occurs in a thin levee mud unit that rests directly on the top of the mass transport unit. No *P. obliquiloculata* was found above the mass-transport unit at Site 944, although the isotopic character of the section immediately above the mass transport unit is similar in Sites 936 and 944 (i.e., a gradual decrease downcore in $\delta^{18}O$ to a value of –0.5‰; Showers et al., this volume). At all three sites, sediment recovery in the cores a few tens of meters above the MTD was poor because of the presence of sandy HARPs. Although the presence of *P. obliquiloculata* and isotopic data are only of stratigraphic value within a particular glacial cycle, seismic correlation with Sites 942 and 946 suggests that the sediment over URMTD is considerably younger than the last interglacial (Stage 5). Furthermore, experience at Sites 935, 936, 944, and 946 is that recovery was good in highstand carbonate clays; none were recovered above the URMTD.

The evidence for the maximum age of overlying sediment is clearest at Site 936, where no more than 4 m of stratigraphic section is missing between the MTD and the overlying autochthonous sedi-

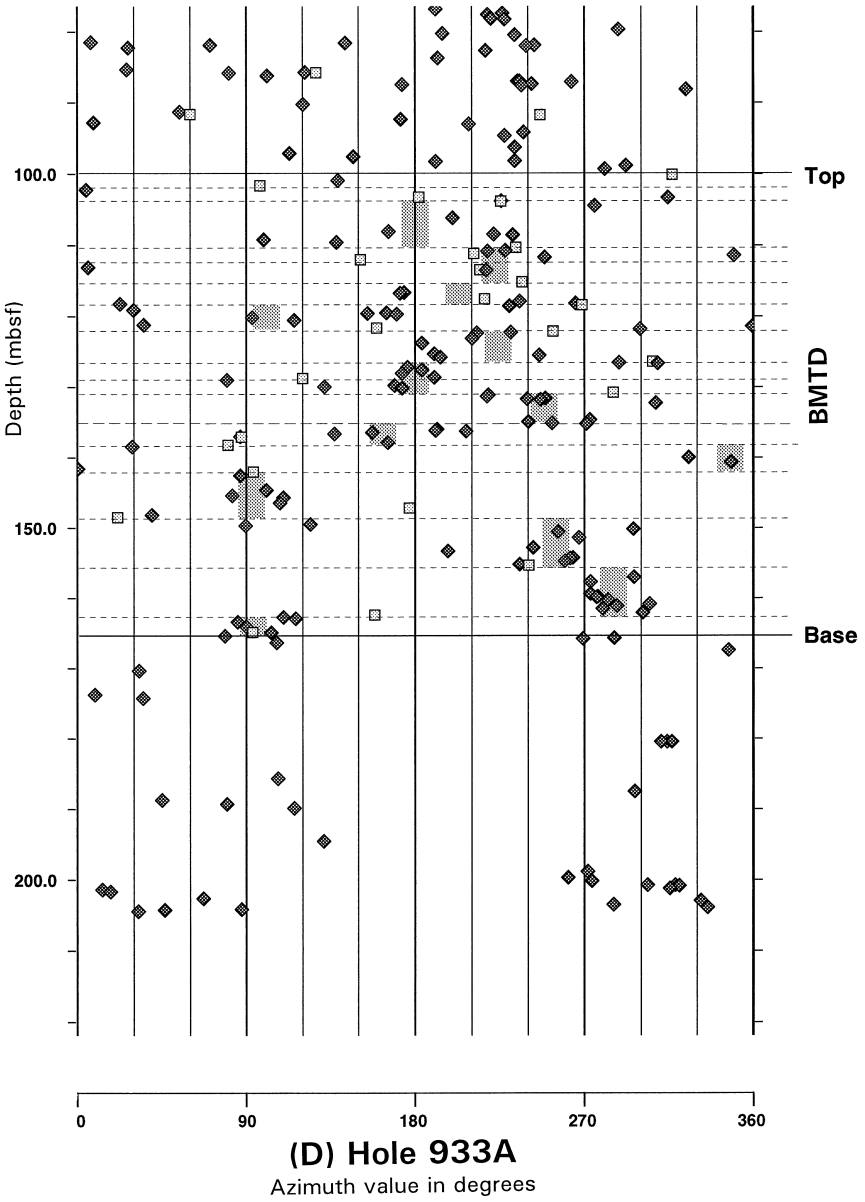

Figure 21 (continued).

ments (Fig. 3). Unless there is a remarkable hiatus on top of the URMTD, then the maximum age of the sediment overlying the URMTD is ~80 ka, because neither sediment nor isotopic values typical of isotopic Stage 5 have been recovered above the URMTD. A maximum age of ~50 ka seems likely if a reasonable sedimentation rate is assumed for the sediment between the *P. obliquiloculata* datum and the URMTD (see also Maslin and Mikkelsen, this volume).

At Site 936, the mass-transport unit rests on ~10 m of levee mud and silt, that in turn overlies a thick sequence of sandy turbidite beds from isotopic Stage 6 in the Red Channel-levee System. At Site 944, the MTD also rests on levee muds of the Red System. In contrast, at Site 935 the URMTD rests on 10 m of levee mud and silt overlying carbonate-rich highstand sediment that Maslin and Mikkelsen (this volume) interpret as isotopic Stage 9. Seismic-reflection profiles (Flood, Piper, Klaus, et al., 1995, "Site 934" chapter, fig. 34) suggest that the eastern levee crest has been eroded, but no erosion is resolved at the western crest at site 934.

At Site 930, an MTD underlies the levee-crest sediment of the Orange Channel-levee System (see fig. 17 of Pirmez and Flood, 1995). The *P. obliquiloculata* marker is 50 m above the top of the MTD, suggesting that the stratigraphic position of this deposit may be identical to the URMTD at other sites. Seismic correlation indicates that this MTD occurs within the Orange-1 Levee (Pirmez and Flood, 1995), in which case it would be younger than URMTD.

Nannofossil-bearing clasts in URMTD at Site 944 are from Zone CN15, at Site 936 from Zone CN15a and at Site 935, where the base of the deposit cuts down into older sediment, from both CN15a and CN14b (the latter both near the base of the flow and 50 m above the base of the flow).

The hiatus between recovered autochthonous sediment above and below the URMTD thus extends from ~50 ka (Site 936) to at least 130 ka (because there is neither lithologic nor isotopic evidence for recovery of Stage 5 deposits, and in particular Stage 5e calcareous clays, at any site beneath the URMTD). The restriction of CN14b calcareous clasts to Site 935, which is the only site where the deposit directly overlies CN14b sediment, suggests that these old clasts are more likely the result of basal erosion during emplacement than derivation from old sediment in the source area on the continental slope.

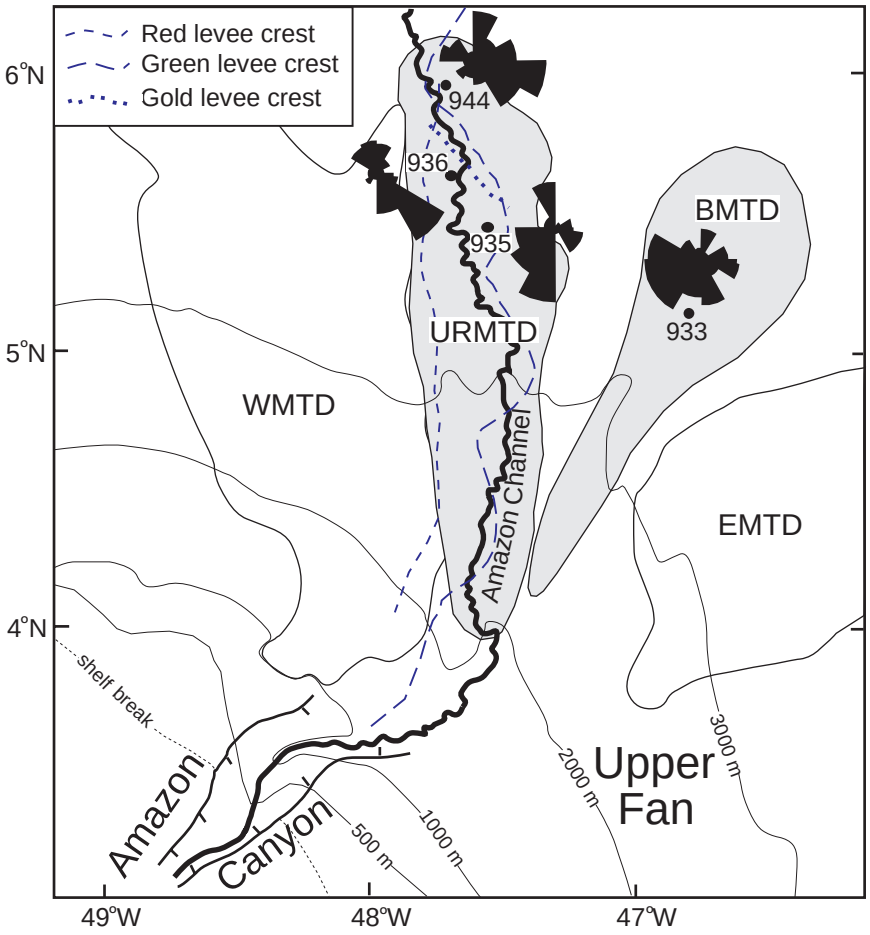

Figure 22. Map of Amazon Fan showing regional variation in azimuths of bedding dips in the WMTD, URMTD, and BMTD. Also shows location of the Yellow, Red, and Green levee crests (cf. Table 1).

Bottom Mass-Transport Deposit

At Site 931, the MTD is overlain by the Channel 5 levee deposit and its underlying HARP, together with ~50 m of older HARPs. The 32 ka Lake Mungo magnetic excursion is ~180 m above the top of the deposit (Fig. 3). At Site 933, the MTD is overlain by levee deposits of the Channel 5 and 6 Systems, with the Lake Mungo Excursion 17 m above the top of the deposit. The lack of HARPs at Site 933 makes this site of greater stratigraphic value. The *P. obliquiloculata* marker was not recognized in either site, and Maslin and Mikkelsen (this volume) therefore interpret the BMTD as younger than the URMTD. At Sites 932 and 938, however, where there is a better foraminiferal record, the *P. obliquiloculata* marker occurs above the Channel 6 deposits. Seismic correlation therefore suggests that the top of the BMTD is considerably older than the *P. obliquiloculata* marker and could be the same age as the URMTD.

At both sites, the MTD rests directly on highstand carbonate clay correlated with isotopic Stage 7 (Maslin and Mikkelsen, this volume) resting on the crest of the Bottom Levee Complex. Rare nannofossil-bearing clasts at Site 931 are from Zone CN15a.

DISCUSSION

Age

The best estimates for the age of the surficial MTDs come from isotopic determinations on foraminifers in piston cores. The WMTD dates from near the last glacial maximum. The EMTD is overlain by some Stage 3 sediments (Fig. 29) and is thus a little older than the WMTD, even though it appears fresher (more distinct contrast in acoustic backscatter) and more blocky on GLORIA imagery. The MTD at 50°W is probably composite; part predates isotopic Stage 3.3, but part may be of the same age as the WMTD.

At least the upper part of the URMTD dates from ~45 ka and of the BMTD from ~37 ka, although within the limits of resolution of bio- and magnetostratigraphy, these two deposits could be synchronous. Older MTDs are difficult to recognize in the seismic-reflection profiles (but note deposit below the Bottom Levee Complex illustrated in fig. 23.6 of Flood et al., 1991).

Does the pronounced age gap in at least the buried MTDs indicate that they represent multiple events that occurred over a long period of time? Or is the age gap a result of basal erosion by the flow? Seismic-reflection profiles generally do not show stratified sediment interbedded with the MTDs, and the margins of the deposits do not have multiple snouts interbedded with stratified sediments. The distribution of clasts in the URMTD is consistent with erosion at the base of the flow. Seismic-reflection profiles show that the surface of the Bottom Levee Complex is locally quite irregular (Flood, Piper, Klaus, et al., 1995, "Site 933" chapter, fig. 2) and may be indicative of erosion; clay mineralogy of clasts within the BMTD also suggests some erosion.

Source

Two hypotheses have been considered for the source of the MTDs. Some of the seismic-reflection data suggests that the MTDs represent channel-levee sediment that has deformed essentially in situ (parautochthonous model). In contrast, on the basis of microfos-

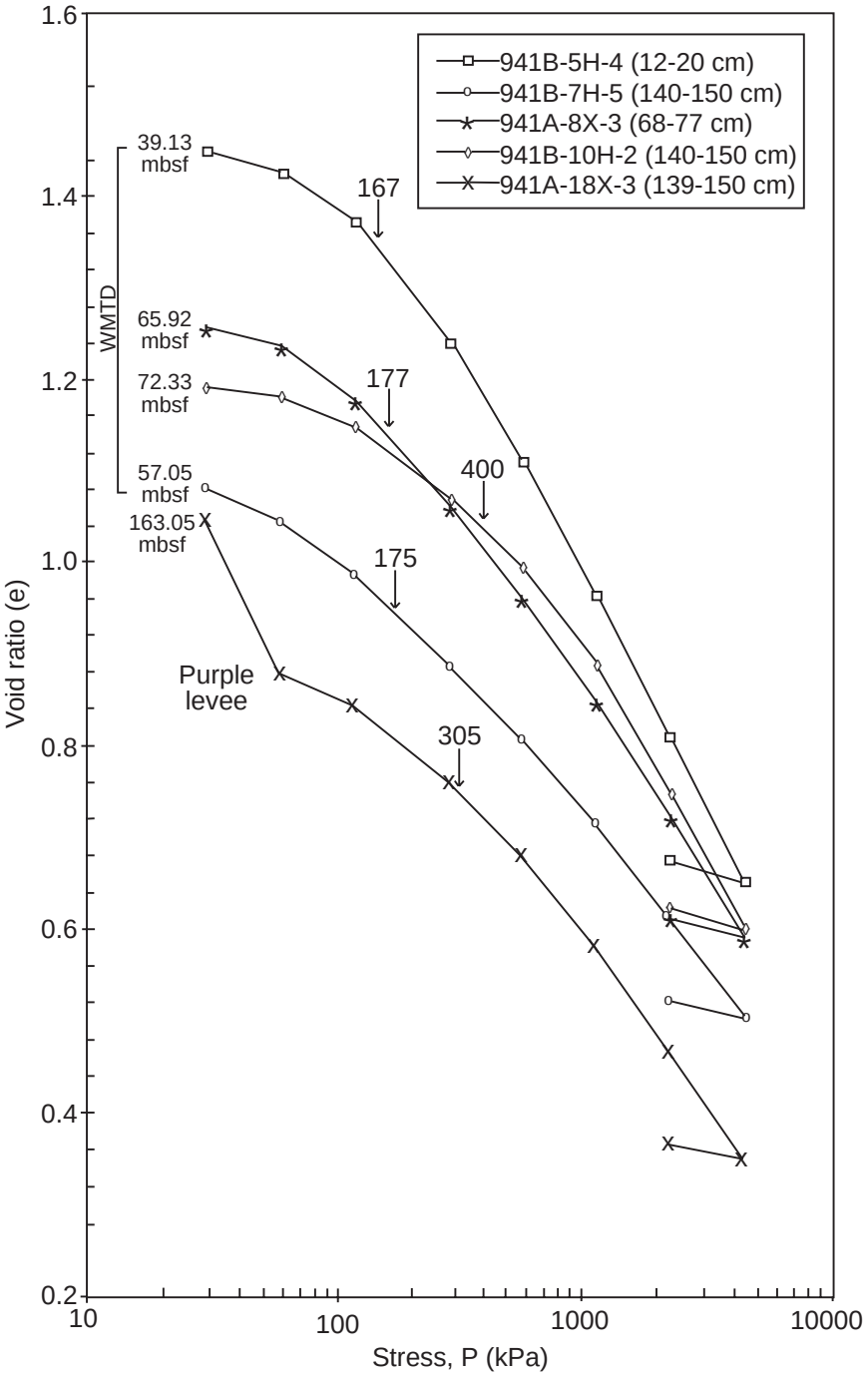

Figure 23. Oedometer consolidation tests from Site 941. Arrows indicate *Pc′* values.

sils, Vilela and Maslin (this volume) conclude that the MTDs were initiated in middle to upper bathyal depths with rare shelf contributions.

Evidence supporting the interpretation of a parautochthonous origin for the MTD includes the following: (1) The incorporation of carbonate-rich interglacial sediment at the base of Site 931 and locally within Site 935 and Site 944. These calcareous clay deposits lack bathyal benthic foraminifers and are therefore unlikely to have been transported from the continental slope. (2) Some blocks are lithologically similar to fine-grained levee deposits. In particular, a distinctive clay mineral occurs in some blocks near the base of the BMTD in Site 931 and the underlying levee, but nowhere else (Debrabant et al., this volume). (3) At some sites, a few microfossil samples are barren of bathyal benthic foraminifers and contain rare abyssal benthic foraminifers. These blocks presumably originated in abyssal water depths (Fig. 30). (4) There is a downfan increase in the proportion of sand in the buried MTDs that parallels a downfan increase in the proportion of sand in levee sediment (Manley et al., this volume). (5) The total volume of the surficial MTDs appears greater than the "missing" sediment inferred from seismic-reflection profiles of the source areas.

Most of the authors of this report feel that the bulk of the evidence supports an interpretation that most of the sediment in the MTDs was derived from channel-levee deposits in water depths of 500 to 2000 m on the continental slope. By analogy with the WMTD, some of this sediment was derived directly from failure on the continental slope

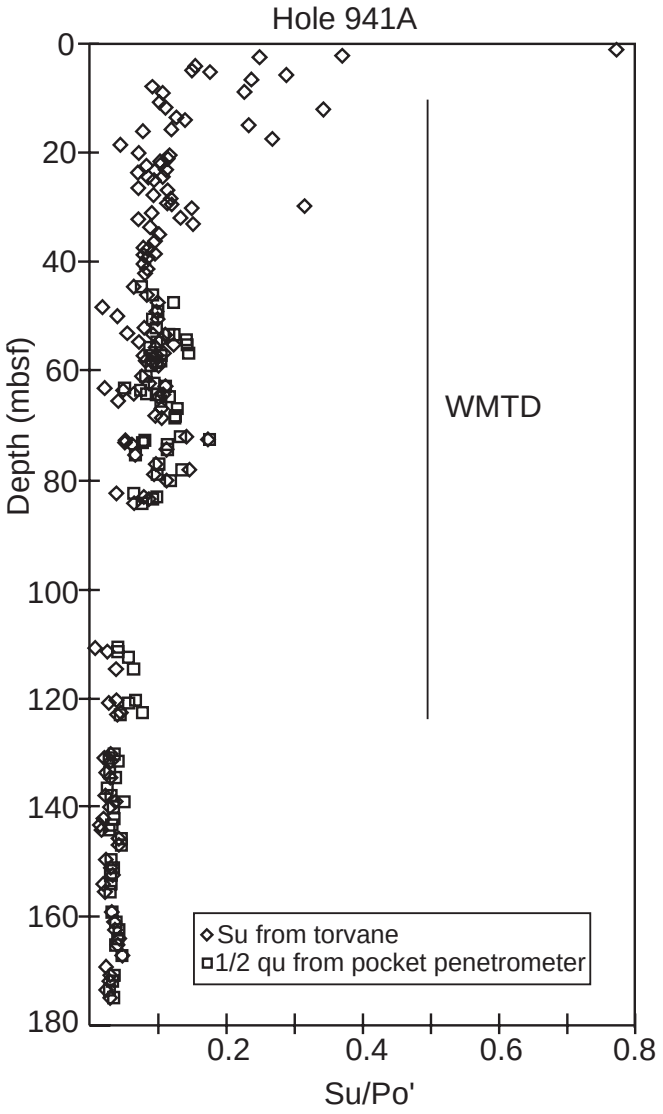

Figure 24. Plot of ratio of undrained shear strength (*Su*) to estimated overburden effective stress (*Po'*) against depth for Site 941. Shows wide scatter in upper part of WMTD, suggesting that the strengths of clasts and matrix are very variable.

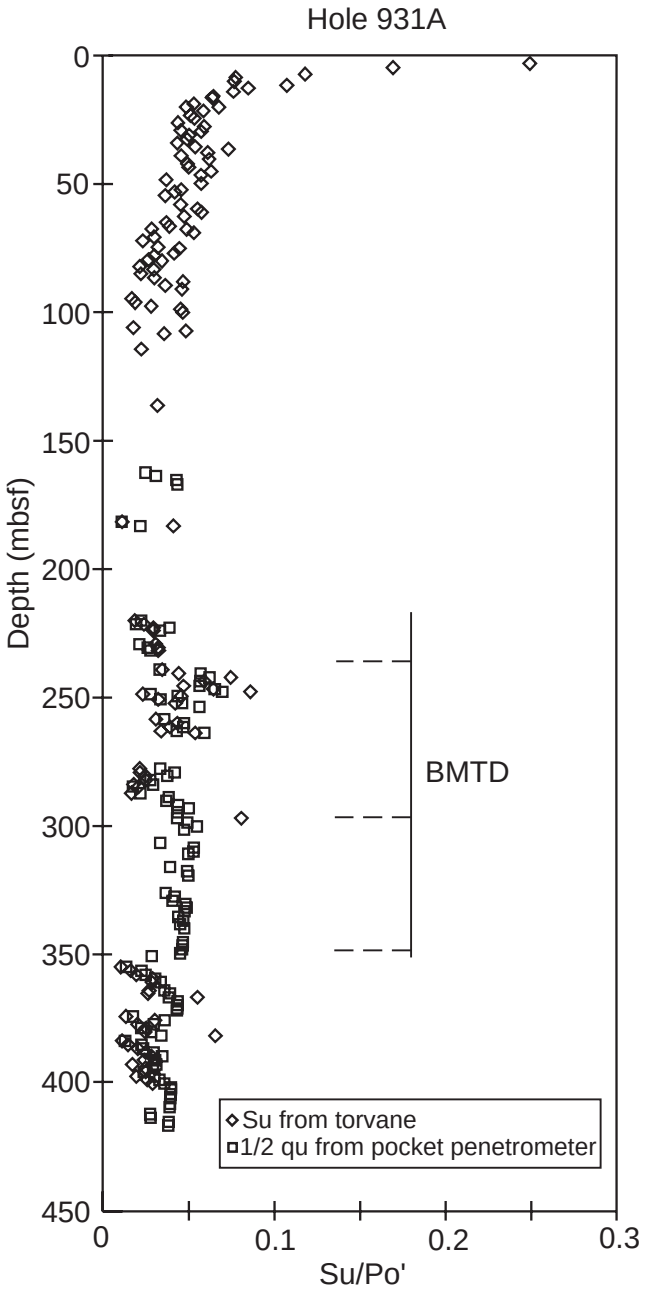

Figure 25. Plot of ratio of undrained shear strength (*Su*) to estimated overburden effective stress (*Po'*) against depth for Site 931, showing elevated values within the MTD. Dashed lines indicate boundaries in physical properties within the BMTD, discussed in text.

and some from erosion beneath the proximal part of the MTD. Benthic foraminifer abundance is consistently greater in the MTDs compared with levee deposits (see individual site biostratigraphy tables in Flood, Piper, Klaus, et al., 1995), an observation confirmed by the detailed work of Vilela and Maslin (this volume). This suggests the source was in shallower water than the sediment cored during Leg 155. This interpretation is supported by the presence of rare outer shelf foraminifers in a few samples (Vilela and Maslin, this volume). There is no evidence, however, that shelf sediment represents a significant component of the MTDs. The upslope limit of the mapped deposits (Fig. 1) probably corresponds to the predominant source area.

The source of sediment in the MTDs was lithologically complex. At Site 941, intervals of glacial and interglacial sediment blocks alternate, and some smaller clasts are as old as early Miocene, probably brought near the surface by the diapirs within the source region of the WMTD. In all MTDs, carbonate-rich muds are easily recognized as being of different lithology from most clasts, but there is also considerable variability in the color and grain size of mud clasts. Carbonate-rich muds are of variable age.

The folded muds with silt laminae at the top of Sites 931 and 935 contain a "warm glacial" planktonic foraminiferal assemblage with common *P. obliquiloculata* but sparse *G. ruber*. The low degree of compaction of this sediment suggests that it was not deeply buried before failure and therefore probably represents sediment that accumulated between 85 ka and the time of failure. The uniform mud intervals at the base of Sites 933 and 935 and correlative muds in 931 and 936 have an interglacial planktonic foraminiferal assemblage; whether these date from Stage 5 or older sediment is uncertain. Sed-

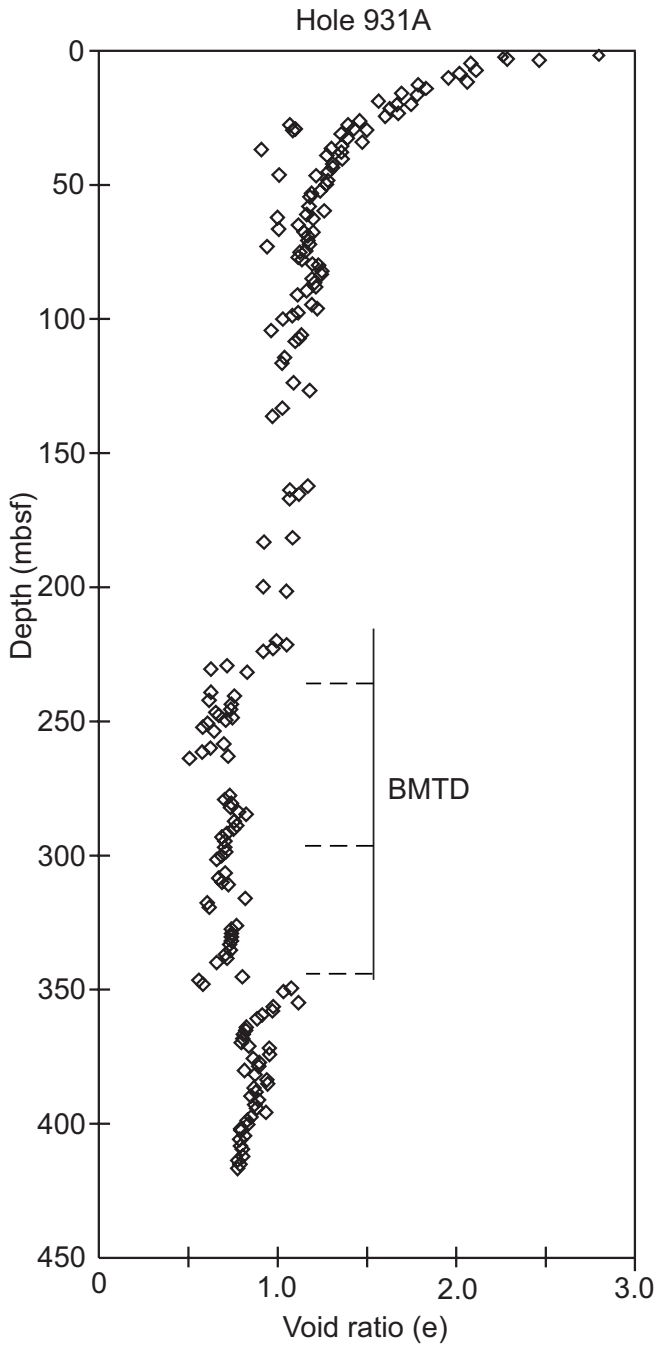

Figure 26. Void ratio plot for Site 931. The BMTD shows as an offset to the left.

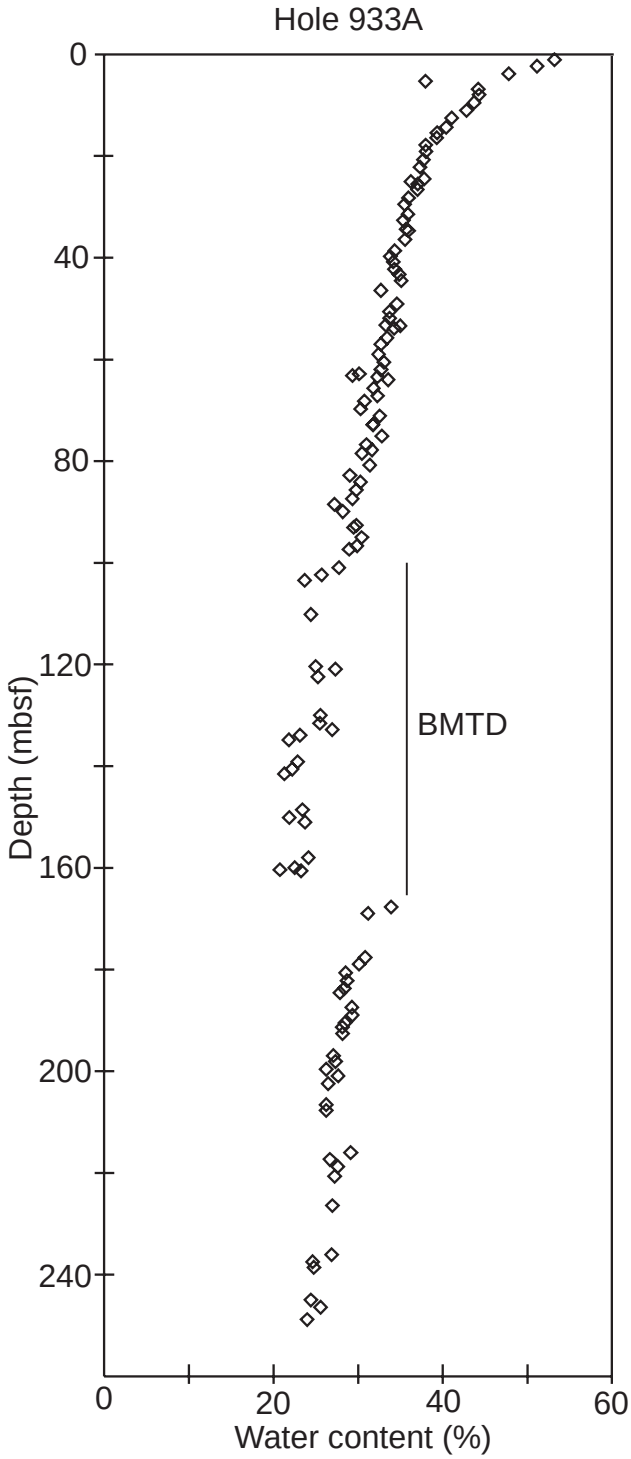

Figure 27. Water content plot for Site 933. The BMTD shows as an offset to the left.

iment in the upper part of Sites 931, 933, 935, and 944 and the middle parts of Site 936 have glacial planktonic foraminiferal assemblages (Fig. 30). Block size is commonly smaller than for the interglacial mud intervals, and more sand and wood fragments are reported in the visual core descriptions. The presence of sand and silt interbeds probably reduces the ability of blocks to remain intact as they are translated.

Figure 30 shows the inferred principal sources of blocks, based mainly on their microfossil assemblages, and the apparent correlation between URMTD and BMTD. The grain-size data of Manley et al. (this volume) show some correlation between inferred source and modal grain size. If only muddy samples (mode > 6ϕ) are considered, the mean modal size of interglacial muds is 7.44ϕ, of "warm glacial" muds is 7.31ϕ, and "cold glacial" muds is 7.28ϕ.

The variation in sediment type and foraminiferal assemblages in the five sites penetrating the URMTD and BMTD can be correlated between sites (Fig. 30). This suggests that there were four phases of sediment supply to the buried MTDs. The first is represented only in Sites 944 and the lower part of URMTD in Site 936, with sandier sed-

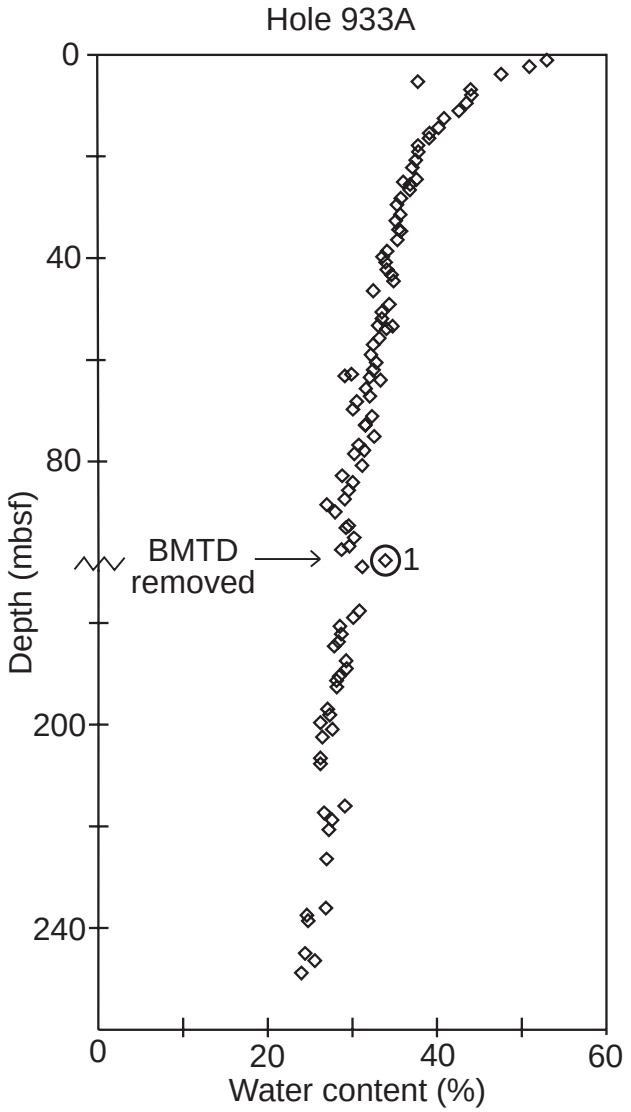

Figure 28. Water content for Site 933 with the MTD removed. This shows the trend above and below the MTD, with a single sample (1) from the overpressured unit beneath the MTD.

iment reaching Site 944. The second is represented by the upper part of Site 936, the lower part of Site 935, the middle part of Site 931, and most of Site 933. The third is represented by the upper part of Site 931 and the extreme top of Site 933. The fourth phase consists of mixed sediment types at the top of Sites 936, 935, and 931 (Fig. 30). There is no evidence for any extended time period between these phases, which are interpreted as representing different source sediment in the failure zone. The lithologic correlation supports the interpretation based on seismic-reflection profiles that the URMTD and BMTD are correlative.

Transport Process

In trying to infer transport processes, we must consider whether different mass-flow units experienced different transport processes and whether individual MTDs resulted from multiple events, perhaps involving different processes. All the MTDs that were cored are in similar water depths on the fan (3346–3701 mbsl) and their similarities in lithology and seismic character suggest that they experienced similar transport processes.

The main transport process appears to have been as a slide of large blocks (meters to decameters) with deformation taken up by relatively small amounts of matrix and by weaker blocks (Fig. 31). The low surface slope of the deposit (<1:100) confirms the presence of some weak matrix or shear surfaces. Matrix-rich deposits with small clasts are common near the top of some units. These may be true debris flows and may also be represented at the snout of the WMTD (Flood, Piper, Klaus, et al., 1995, "Site 941" chapter, fig. 4). The general tendency for the largest and most consolidated blocks to be near the base of the MTDs suggests that the deposits represent either a single event, or a major slope failure followed by lesser retrogressive failures in the slide scar area. The headscarp for the WMTD (Fig. 4) is 120 m high. The degree of consolidation of transported blocks in all the MTDs is consistent with derivation from failure involving this order of sediment thickness.

The strong evidence for the transport of large blocks from bathyal depths on the continental slope needs to be reconciled with the local evidence for erosion at the base of the MTDs and incorporation of abyssal sediment. The distribution of surficial MTDs suggests that they flow between and are commonly bounded by old levee crests. Where the trend of levee crests is locally oblique to the regional fan gradient (e.g., such as in the surface Amazon Channel immediately downslope from Sites 930 and 936, near the Aqua and Brown avulsions), ponding of MTD by the levee may have induced failure in the rapidly deposited levee sediment, which then became incorporated in the mass flow deposit. Such a process would account for the apparent "planing off" of the levee crest at Site 935.

Initiation Process

Several possible hypotheses might account for the triggering of the mass-transport events. On the basis of largely circumstantial evidence, we think that the most probable is that the events are triggered by gas hydrate decompression and sublimation during falling sea level (Kayen and Lee, 1991). On other continental margins, large slides have been triggered by canyon-channel incision during falling sea level (Posamentier et al., 1988) or by rare seismic events unrelated to changes in sea level or channel pattern (Piper et al., 1985). In every case, diapirism may promote sediment instability. The age of the MTDs thus becomes critical for the interpretation of initiation of movement.

The age and source area of the WMTD is best known. It was derived from an old channel-levee deposit, that is disturbed by diapirs (probably of mud). There is a bottom-simulating reflector in the source area of the WMTD and gas hydrates appear to have been present in the WMTD at Site 941 (Soh, this volume). The age of the deposit is not sufficiently constrained to determine unequivocally whether the event took place during falling or rising sea level, although an age synchronous with or immediately preceding the last glacial maximum seems likely. The EMTD was deposited during the progressive fall in sea level during isotopic Stage 3 (Fig. 32).

The ages of the URMTD and BMTD are not sufficiently constrained to determine if there is a correlation with sea-level change. If the MTDs were essentially a single event, as argued above, then their likely age in the early part of isotopic Stage 3 was during a progressive fall in sea level (Fig. 32).

The apparent source areas of the surficial MTDs are separate from the incised Amazon Canyon, and their initiation is thus unlikely to have been triggered by canyon incision. There is no independent evidence for seismic shaking in either the source areas or the continental slope areas unaffected by the MTDs, so that seismic initiation also appears unlikely. On the other hand, the presence of low chlorinity anomalies in some MTDs may be evidence of the presence of gas hydrates in the failed sediment.

CONCLUSIONS

1. At least four major MTDs are recognized on Amazon Fan in the last 100,000 years. Each extends over an area of order of 10^4 km^2 and has a volume of order 10^3 km^3.

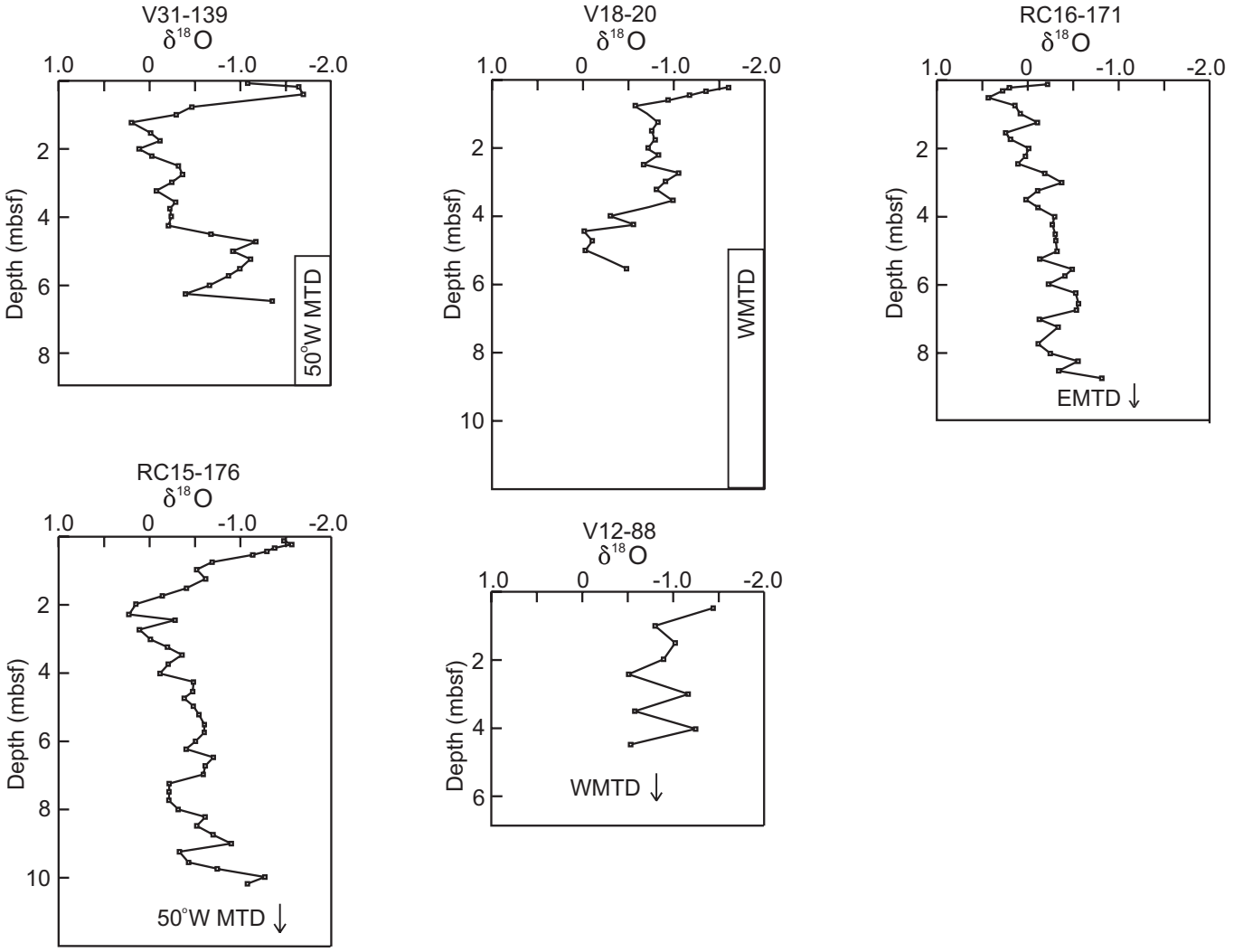

Figure 29. Oxygen isotope determinations and numbers of *G. sacculifer* from piston cores from the WMTDs and EMTDs and the MTD at 50°W. Position of MTD in cores based on Damuth and Embley (1981).

2. Mass-transport events initiated in slope and upper-fan levee sediments, locally steepened by diapiric intrusion and underconsolidated because of rapid prodeltaic deposition during marine lowstands and because of the presence of shallow gas and gas hydrates. The ages of the mass-transport events may correlate with times of falling sea level, when gas hydrate sublimation would further destabilize sediments.

3. MTDs were partly confined by pre-existing channel-levee topography on the fan. In places, elevated levee deposits were eroded by the mass-transport flow and incorporated in the basal part of the deposit.

4. Sediment properties in the MTDs show a broadly repetitive character. There is no evidence that a long time span is represented by discontinuities in sediment properties in the deposits. Rather, they probably represent retrogressive failure from a slump scar similar to that at the head of the WMTD. Correlation of block lithology between sites suggests that the URMTD and BMTD are remnants of the same composite event.

5. The deposits were emplaced as a slide of large blocks (meters to decameters) with deformation taken up by relatively small amounts of matrix and by weaker blocks. Matrix-rich deposits with small clasts at the top of some units are true debris flows.

ACKNOWLEDGMENTS

We thank all our shipboard colleagues who contributed to the description and analysis of the MTDs, and particularly Jed Damuth for his thoughtful historical perspective. Financial support for the acquisition and interpretation of seismic-reflection data was provided by the U.S. National Science Foundation. Most figures were drafted by Mark Deptuck. The manuscript benefited from reviews by Douglas Masson, Homa Lee, Kate Moran, and Mike Lewis.

REFERENCES

Bugge, T., Belderson, R.H., and Kenyon, N.H., 1988. The Storegga slide. *Philos. Trans. R. Soc. London*, 325:357–388.

Coniglio, M., 1986. Synsedimentary submarine slope failure and tectonic deformation in deep water carbonates, Cow Head Group, western Newfoundland. *Can. J. Earth Sci.*, 23:476–490.

Damuth, J.E., and Embley, R.W., 1981. Mass-transport processes on the Amazon Cone: western equatorial Atlantic. *AAPG Bull.*, 65:629–643.

Damuth, J.E., Flood, R.D., Kowsmann, R.O., Belderson, R.H., and Gorini, M.A., 1988. Anatomy and growth pattern of Amazon deep-sea fan as revealed by long-range side-scan sonar (GLORIA) and high-resolution seismic studies. *AAPG Bull.*, 72:885–911.

Damuth, J.E., Kowsmann, R.O., Flood, R.D., Belderson, R.H., and Gorini, M.A., 1983. Age relationships of distributary channels on Amazon deep-sea fan: implications for fan growth pattern. *Geology,* 11:470–473.

Embley, R.W., and Jacobi, R.D., 1986. Mass wasting in the western North Atlantic. *In* Vogt, P.R., and Tucholke, B.E. (Eds.), *The Western North Atlantic Region.* Geol. Soc. Am., Geol. of North Am. Ser., M:479–490.

Flood, R.D., Manley, P.L., Kowsmann, R.O., Appi, C.J., and Pirmez, C., 1991. Seismic facies and late Quaternary growth of Amazon submarine fan. *In* Weimer, P., and Link, M.H. (Eds.), *Seismic Facies and Sedimentary Processes of Submarine Fans and Turbidite Systems:* New York (Springer), 415–433.

Flood, R.D., Piper, D.J.W., Klaus, A., et al., 1995. *Proc. ODP, Init. Repts.,* 155: College Station, TX (Ocean Drilling Program).

Gibson, R.E., 1958. The progress of consolidation in a clay layer increasing in thickness with time. *Geotechnique,* 8:71–182.

Hampton, M.A., Lee, H.J., and Locat, J., 1996. Submarine landslides. *Rev. Geophys.,* 34:33–59.

Jacobi, R.D., 1976. Sediment slides on the northwestern continental margin of Africa. *Mar. Geol.,* 22:157–173.

Kayen, R.E., and Lee, H., 1991. Pleistocene slope instability of gas hydrate-laden sediment on the Beaufort Sea Margin. *Mar. Geotechnol.,* 10:125–141.

Kenyon, N.H., 1987. Mass-wasting features on the continental slope of northwest Europe. *Mar. Geol.,* 74:57–77.

Lee, H.J., 1989. Undersea landslides: Extent and significance in the Pacific Ocean. *In* Brabb, E.E., and Harrod, B.L. (Eds), *Landslides: Extent and Economic Significance.* Proc. 28th Int. Geol. Congr., Rotterdam (Balkema), 367–379.

Manley, P.L., and Flood, R.D., 1988. Cyclic sediment deposition within Amazon deep-sea fan. *AAPG Bull.,* 72:912–925.

Masson, D.G., Huggett, Q.J., and Brunsden, D., 1993. The surface texture of the Saharan debris-flow deposit: some speculations on submarine debris-flow processes. *Sedimentology,* 40:583–598.

Middleton, G.V., and Hampton, M.A., 1976. Subaqueous sediment transport and deposition by sediment gravity flows. *In* Stanley, D.J., and Swift, D.J.P. (Eds.), *Marine Sediment Transport and Environmental Management:* New York (Wiley), 197–218.

Moran, K., Brückmann, W., Feeser, V., and Campanella, R.G., 1993. In-situ stress conditions at Nankai Trough, Site 808. *In* Hill, I.A., Taira, A., Firth, J.V., et al., *Proc. ODP, Sci. Results,* 131: College Station, TX (Ocean Drilling Program), 283–291.

Nardin, T.R., Hein, F.J., Gorsline, D.S., and Edwards, B.D., 1979. A review of mass movement processes, sediment and acoustic characteristics, and contrasts in slope and base-of-slope systems versus canyon-fan-basin floor systems. *In* Doyle, L.J., and Pilkey, O.H. (Eds.), *Geology of Continental Slope*. Spec. Publ.— Soc. Econ. Paleontol. Mineral., 27:61-73.

Normark, W.R., 1990. Return to Ranger submarine slide, Baja California, Mexico. *Geo-Mar. Lett.,* 10:81–91.

Normark, W.R., and Gutmacher, C.E., 1988. Sur submarine slide, Monterey Fan, central California. *Sedimentology,* 35:629–647.

Piper, D.J.W., Farre, J.A., and Shor, A.N., 1985. Late Quaternary slumps and debris flows on the Scotian Slope. *GSA Bull.,* 96:1508–1517.

Piper, D.J.W., Panagos, A.G., and Pe, G.G., 1978. Conglomeratic Miocene flysch, western Greece. *J. Sediment. Petrol.,* 48:117–126.

Pirmez, C., 1994. Growth of a submarine meandering channel-levee system on the Amazon Fan [Ph.D. thesis]. Columbia Univ., New York.

Pirmez, C., and Flood, R.D., 1995. Morphology and structure of Amazon Channel. *In* Flood, R.D., Piper, D.J.W., Klaus, A., et al., *Proc. ODP, Init. Repts.,* 155: College Station, TX (Ocean Drilling Program), 23–45.

Posamentier, H.W., Jervey, M.T., and Vail, P.R., 1988. Eustatic controls on clastic deposition, I. Conceptual framework. *In* Wilgus, C.K., Hastings, B.S., Ross, C.A., Posamentier, H.W., Van Wagoner, J., and Kendall, C.G.St.C. (Eds.), *Sea-Level Changes: An Integrated Approach.* Spec. Publ.—Soc. Econ. Paleontol. Mineral., 42:109–124.

Prior, D.B., Bornhold, B.D., and Johns, M.W., 1984. Depositional characteristics of a submarine debris flow. *J. Geol.,* 92:707–727.

Skempton, A.W., 1970. The consolidation of clays by gravitational compaction. *Q. J. Geol. Soc. London,* 125:373–411.

Terzaghi, K., and Peck, R.B., 1967. *Soil Mechanics in Engineering Practice* (2nd ed.): New York (Wiley).

Trincardi, F., and Normark, W.R., 1989. Pleistocene Suvero slide, Paola Basin, southern Italy. *Mar. Pet. Geol.,* 6:324–335.

Varnes, D.J., 1978. Slope movement types and processes. *In* Schuster, R.L., and Krizek, R.J. (Eds.), *Landslides: Analysis and Control.* U.S. Nat. Res. Counc., Trans. Res. Bd. Spec. Rep., 176:12–33.

Walker, J.R., and Massingill, J.V., 1970. Slump features on the Mississippi Fan, northern Gulf of Mexico. *GSA Bull.,* 81:3101–3108.

Date of initial receipt: 15 December 1995
Date of acceptance: 17 May 1996
Ms 155SR-212

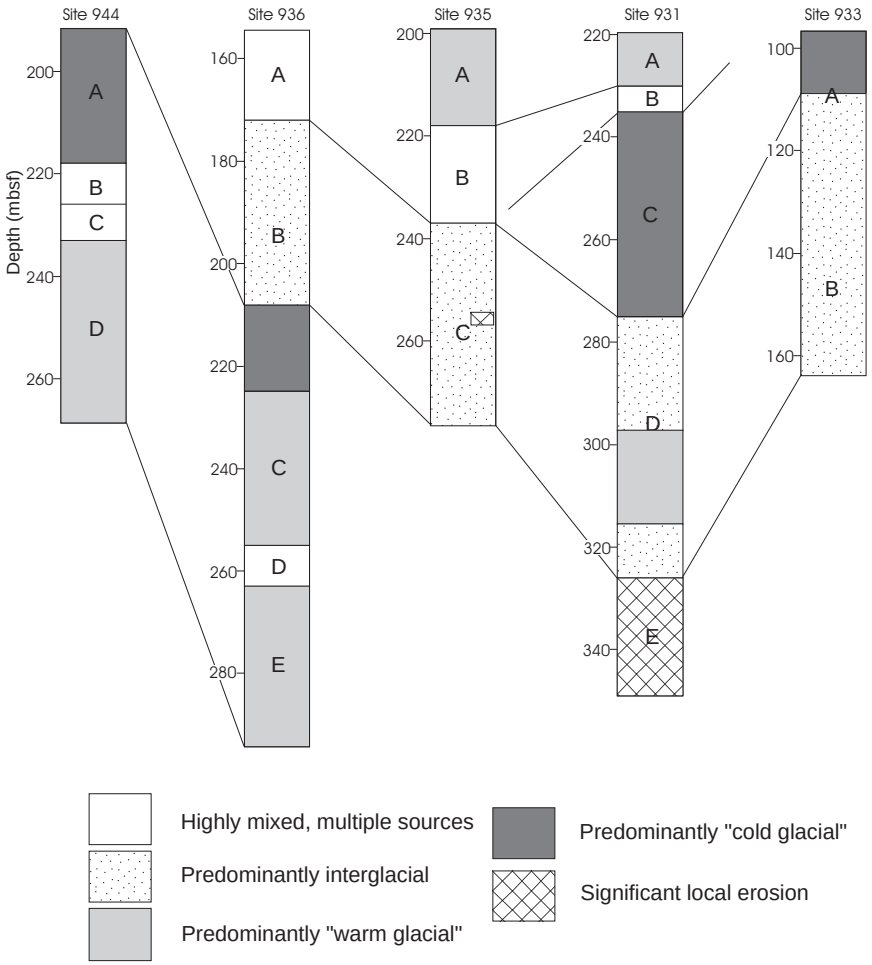

Figure 30. Inferred age of source sediment and probable correlation of transported sediment within the URMTD and BMTD, keyed to lithology summary in Figure 14.

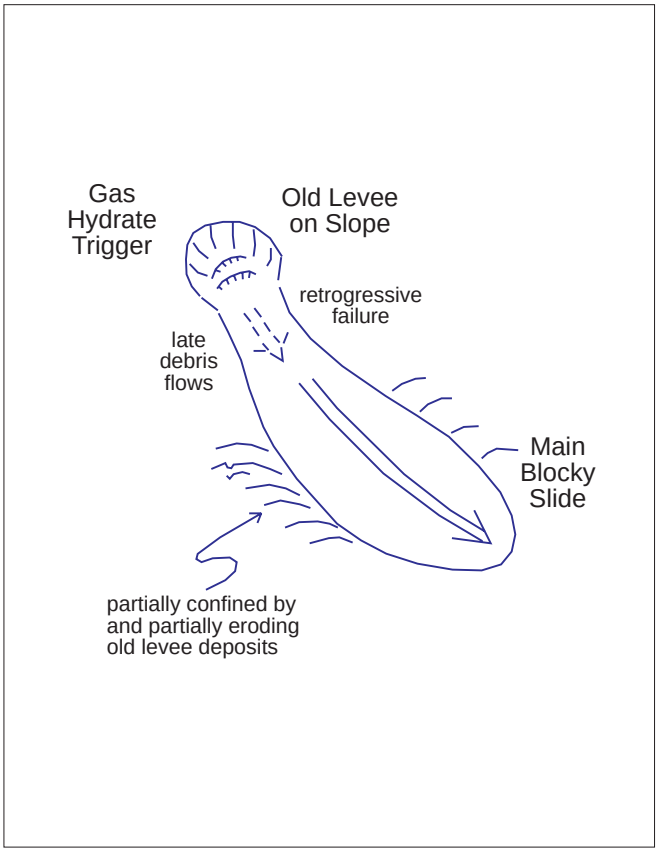

Figure 31. Drawing illustrating source and flow of MTDs on Amazon Fan.

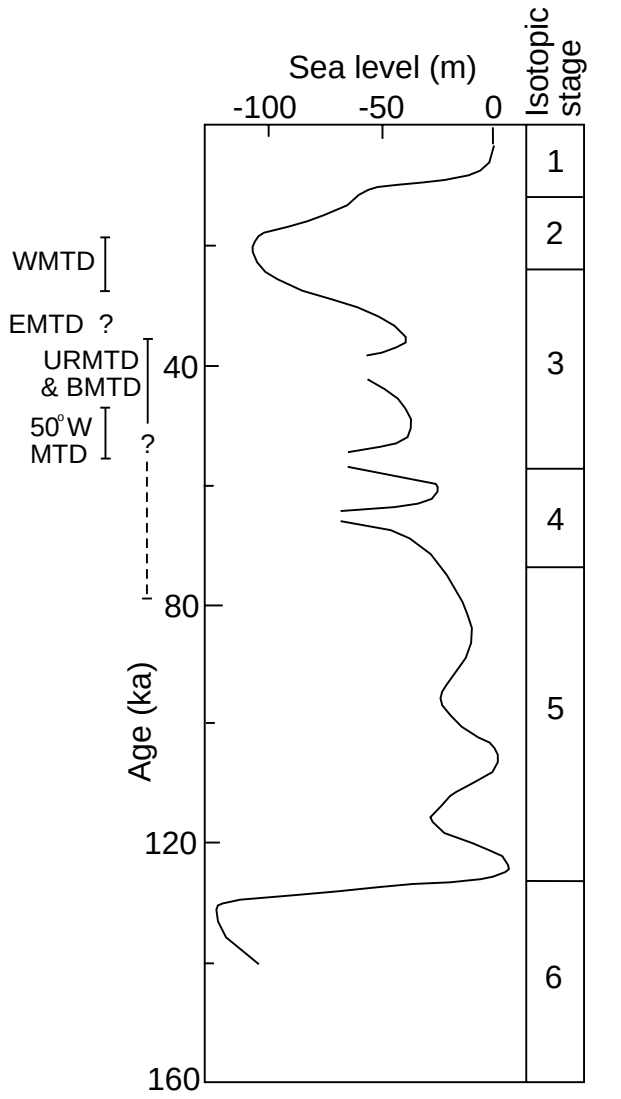

Figure 32. Age of MTDs plotted against sea-level curve (from Flood, Piper, Klaus, et al., 1995, “Introduction” chapter, fig. 7).

Previous Chapter Table of Contents Next Chapter